2011

Active disturbance rejection for the bipedal walk of a humanoid robot using the motion of the arms

Joshua Hill

ACTIVE DISTURBANCE REJECTION FOR THE BIPEDAL WALK OF A HUMANOID ROBOT USING THE MOTION OF THE ARMS

by

JOSHUA HILL

A THESIS

Submitted in partial fulfillment of the requirements
for the degree of Master of Science in Engineering
in
The Department of Mechanical and Aerospace Engineering
to
The School of Graduate Studies
of
The University of Alabama in Huntsville

HUNTSVILLE, ALABAMA

2011

In presenting this thesis in partial fulfillment of the requirements for a master's degree from The University of Alabama in Huntsville, I agree that the Library of this University shall make it freely available for inspection. I further agree that permission for extensive copying for scholarly purposes may be granted by my advisor or, in his/her absence, by the Chair of the Department or the Dean of the School of Graduate Studies. It is also understood that due recognition shall be given to me and to The University of Alabama in Huntsville in any scholarly use which may be made of any material in this thesis.

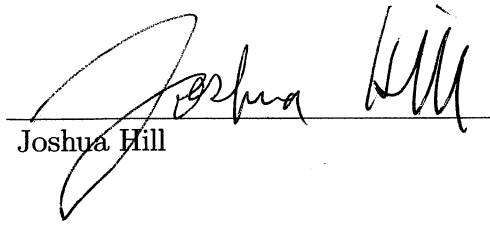

Joshua Hill

12/5/11
(date)

THESIS APPROVAL FORM

Submitted by Joshua Hill in partial fulfillment of the requirements for the degree of Master of Science in Engineering in Mechanical Engineering and accepted on behalf of the Faculty of the School of Graduate Studies by the thesis committee.

We, the undersigned members of the Graduate Faculty of The University of Alabama in Huntsville, certify that we have advised and/or supervised the candidate of the work described in this thesis. We further certify that we have reviewed the thesis manuscript and approve it in partial fulfillment of the requirements for the degree of Master of Science in Engineering in Mechanical Engineering.

Dr. Farbod Fahimi	11/1/2011 (Date)	Committee Chair
Dr. Nathan J. Slegers	11/1/2011 (Date)	
Dr. Yuri B. Shtessel	11/01/2011 (Date)	
Dr. Keith Hollingsworth	11/1/11 (Date)	Department Chair
Dr. Shankar Mahalingam	11/01/11 (Date)	College Dean
Dr. Rhonda Kay Gaede	12/5/11 (Date)	Graduate Dean

ABSTRACT

School of Graduate Studies
The University of Alabama in Huntsville

Degree Master of Science in Engineering College/Dept. Engineering/Mechanical and Aerospace Engineering

Name of Candidate Joshua Hill

Title Active Disturbance Rejection for the Bipedal Walk of a Humanoid Robot Using the Motion of the Arms

The swing phase of an 18-DOF biped humanoid robot is considered. The robot consists of 12-DOF for the body and legs, and 6-DOF for the arms. It is to follow a stable walking gait, even in the event of a bounded disturbance. The robot mitigates the disturbance by compensating with the acceleration of the arm joints. It is assumed that force sensors exist on the bottom of the robot's feet that provide real-time feedback of the robot's support forces and moments. Additionally, the servo motors at the joints provide position, velocity, and acceleration information for feedback. A sliding mode methodology is used for the disturbance rejection control system. This control system uses the acceleration of the arm joints to maintain the desirable support forces and moments that create the stable walking gait. Through simulations via MATLAB's Simulink program, it can be demonstrated that the proposed disturbance rejection controller is successful.

Abstract Approval: Committee Chair

Dr. Farbod Fahimi

Department Chair

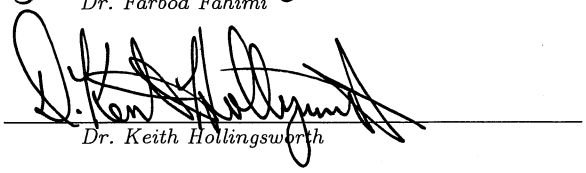

Dr. Keith Hollingsworth

Graduate Dean

Dr. Rhonda Kay Gaede

ACKNOWLEDGMENTS

I would like to thank my advisor, Dr. Farbod Fahimi for giving me the opportunity to do research on humanoid robots. His guidance and advice enabled me to successfully complete my thesis. I would also like to thank Charles Boyles for his assistance in creating the CAD model of the BIOLOID robot, and for his many other contributions. I'm additionally grateful for the technical support team at Mathworks for assisting me with Matlab coding troubles. Most importantly, I would like to thank my family, especially my fiance Lisa Friederich, for supporting me morally and financially during my graduate studies.

TABLE OF CONTENTS

LIST OF FIGURES

LIST OF TABLES

LIST OF SYMBOLS

SYMBOL	DEFINITION
a_i	Denavit-Hartenburg length parameter for link i
$\mathbf{C}$	Matrix with damping coefficients
d_i	Denavit-Hartenburg offset parameter for link i
$\mathbf{d}$	Unknown actual disturbance vector
$\mathbf{D}$	Upper bound of actual disturbance vector
$\mathbf{F}_R$	Actual force vector exerted by robot to ground
$\mathbf{F}_R^d(t)$	Desired force vector exerted by robot to ground
$\mathbf{F}_s$	Actual force vector exerted by ground to robot
F_x	Vertical support force
F_y	Lateral support force
F_z	Longitudinal support force
$\mathbf{g}$	Gravitational acceleration vector
$\mathbf{G}_{ai}$	Jacobian matrix for arm joint angular velocities
$\mathbf{G}_{bi}$	Jacobian matrix for body/legs joint angular velocities
$\mathbf{I}_i^B$	Link i moment of inertia matrix expressed in local frame
$\mathbf{J}_{ai}$	Jacobian matrix for arm joint linear velocities

$\mathbf{J}_{bi}$	Jacobian matrix for body/legs joint linear velocities
$\mathbf{K}$	Sliding mode gain matrix
$\mathbf{K}_u$	Gain for the switching controller
$\mathbf{K}_v$	Row vector containing the diagonal elements of $\mathbf{K}$
L	Impulse
m_i	Mass of link i
$\mathbf{M}_R$	Actual moment vector exerted by robot to ground
$\mathbf{M}_R^d(t)$	Desired moment vector exerted by robot to ground
$\mathbf{M}_s$	Actual moment vector exerted by ground to robot
M_x	Support moment about the vertical axis
M_y	Support moment about the lateral axis
M_z	Support moment about the longitudinal axis
N	Number of links in the system
P	Position vector
${}^{i-1}P_{iORG}$	Origin of frame i with respect to frame $i-1$
P_x	Position vector about local x-axis
P_y	Position vector about local y-axis
P_z	Position vector about local z-axis
$\mathbf{q}$	Joint variables of the robot's limbs

$\mathbf{q}_a$	Vector containing arm joint positions
$\mathbf{q}_b$	Vector containing body/legs joint positions
$\mathbf{q}^d(t)$	Desired joint variables of the robot's limbs
$\mathbf{r}_i$	Position vector of the center of gravity of link i
$\mathbf{R}_{0i}$	Transformation from local frame of link i to inertial frame
Rot_x	Transformation matrix for pure rotation about the local x-axis
$\mathbf{s}$	Parameter defining the surface for sliding mode control
t	Time
${}_i^{i-1}T$	Transformation matrix for frame i to frame $i-1$
Trans_x	Transformation matrix for pure translation along the local x-axis
$\mathbf{u}$	Control input - vector containing arm joint accelerations
v	Velocity
V	Lyapunov function
$\hat{X}_i$	X unit vector for link i
$\mathbf{y}$	Actual control output
$\hat{Y}_i$	Y unit vector for link i
$\mathbf{y}^d$	Desired control output
$\mathbf{y}_m$	Measured control output
$\mathbf{z}$	Double time integral of control output

$\hat{Z}_i$	Z unit vector for link i
ZMP	Zero Moment Point
ZMP_y	Zero Moment Point along lateral direction
ZMP_z	Zero Moment Point along longitudinal direction
α_i	Denavit-Hartenburg twist parameter for link i
η	Column vector with positive elements
θ_i	Denavit-Hartenburg angle parameter for link i
$\mathbf{\Lambda}$	Positive definite diagonal square matrix
$\boldsymbol{\omega}_i$	Link i angular velocity vector expressed in global frame
$\boldsymbol{\omega}_i^B$	Link i angular velocity vector expressed in local frame

CHAPTER 1

INTRODUCTION

Humanoid robotics has been a topic of fascination for many researchers for decades. The characteristic bipedal gait of humanoids has, in particular, been the focus of much research. This research can be divided into two broad, yet distinct groups: passive bipeds and active bipeds.

Passive bipeds are those that take advantage of the natural dynamics of the system and require little to no actuation to perform the walking motion, such as is discussed in [1]. Fully passive bipeds are of little practical use, as they usually function off of potential energy to walk down an incline plane. Many passive dynamic walkers (PDW) are relatively simple mechanisms that often require tweaking to perform correctly. They are sensitive to initial conditions and are not robust enough to handle external disturbances. As a result, they are normally the focus of academic studies in the energy efficiency of bipedal walking gaits such as in [2]. This is not to say that passive bipeds are without use. The research into passive bipeds has led to developments in active bipeds where the natural dynamics of the walking gait are used to reduce the consumption of energy normally required to actuate motors [3].

The focus of this thesis however falls into the category of active bipeds, or those that require significant actuation to perform their gait.

Humans are often studied to gain an understanding into the bipedal gait, and are used as inspiration into various control methods that are applied, in particular, to active bipeds [4, 5]. This is because humanoid robots are designed to operate in an environment that is dominated by humans, and therefore an environment that is designed for bipedal walking.

The most popular methods of control for bipedal robots use the concept of Zero Moment Point (ZMP). The ZMP is the point on the ground where all of the forces that act upon the robot can be replaced by a single force that causes the horizontal moment components to equal zero. The support polygon is the area on the ground that is covered by the feet during locomotion. It is a necessary and sufficient condition for the stable dynamic locomotion of the biped for the ZMP to remain inside the support polygon [6]. If the ZMP moves outside of the support polygon, then the robot will become unstable and begin to fall over. The first ZMP-based approach for biped walking control has the ZMP remaining inside the support polygon at all times, as defined by the desired trajectory of the biped joints. This approach has been successfully used for Manus-I [7], and the famous Honda Asimo Robot [8]. This approach has no closed-loop control to ensure that the ZMP stays within the support polygon when an external disturbance occurs. Essentially, the humanoid is given a specific set of joint torques to accomplish a specific task. The humanoid then performs the task following the prescribed torques. Problems occur if the robot encounters something, such as an external disturbance or an uneven

surface, that was not anticipated at the time the joint torques were set. Due to a lack of feedback, the robot will not be able to "sense" the difference in the joint torques. The robot, therefore fails to compensate for the differences and the ZMP could move outside of the support polygon. When this happens, the robot will become unstable and fall in the direction of the ZMP.

The second approach is the incorporation of feedback for ZMP disturbance compensation; disturbances modify the joint trajectories or joint torques in real-time to keep the ZMP within the support polygon.

One example of modifying joint torques is injecting compensating torque into the ankle-joint of the foot of a robot. This modification enhances ZMP control, as demonstrated in [9]. A different method is to control the angular momentum of the robot and adjust it by modifying the joint torques [10, 11].

There have been numerous methods proposed for the modification of joint trajectories for ZMP control, mostly involving modifying the position of joints. A few methods involve varying the step time, stride, or speed of the walk [12–14], however this method can prove problematic for certain situations, such as the stepping stone problem where the biped must step on certain locations. Modification of the humanoid's trunk or waist motion has been studied [15–17], and even exploiting the upper body's natural dynamics in its control [18], has been considered. Modification of the motion of the robot's base link of the stance leg [19] has been introduced as well. Modeling the full dynamics of a humanoid robot involves many complex, coupled, nonlinear equations that are computationally intensive.

As a result of this, it is normal for simplified models of the robot to be used to ease the computational burden. A common method is to model the biped as an inverted pendulum. In [20], this model was for a 30 degree-of-freedom (DOF) biped to manipulate the ZMP indirectly by controlling the center of gravity (COG). In order to provide more naturalness in the biped's walk, a linear inverted pendulum model (LIPM) is used in [21] to simulate a 12 DOF robot with a moving support ZMP references. The moving ZMP reference results in a motion that looks more natural than a ZMP that is kept at the center of the support polygon. The robot implemented separate proportional-integral-derivative (PID) controllers for each leg. The three dimensional LIMP (3D-LIPM) developed by [22] is implemented in [23] on a 27 DOF HanSaRam-VII robot. In this, the legs of the robot are modeled as weightless, telescopic limbs, with the mass concentrated at a single point, and the ZMP is controlled via the control of the center of mass (COM).

Methods that modify the acceleration of joints has been the focus of study in recent years. Maintaining the upper-body task specifications by controlling the ZMP via modifying the torso's acceleration was proposed by [24]. This was tested on the Honda Asimo platform using the recursive Newton-Euler algorithm to model the robot dynamics. The acceleration of the non-contact limbs as a stabilization strategy was conducted by [25]. In this, the 18 DOF robot is described using morphological gathered from motion capture, and direct measurements of human subjects. It is controlled using a sliding mode control framework, developed by [26], to increase robustness and to take into account modeling errors.

The use of the arms to assist stabilization and control has been considered. Park has studied the implicit relationship of arm swing and its effect on the ground reaction force of the stance foot [27]. A more active role is given to both the trunk and arms of the robot in stabilization against external forces in [28]. In this, a proportional-derivative (PD) controller takes information from a force/torque (F/T) sensor, located between the waist and trunk, as the input for the controller. The use of the arms to interact with the environment in the event of disturbances is discussed in [29].

It's evident that the majority of the research in the dynamic stability of humanoid robots focuses on using the ZMP as the stabilization criteria. However if a 3D model is used, the ZMP position only represents at most three support reaction components: one vertical force, one lateral moment component, and one longitudinal moment component. The lateral and longitudinal support forces and the vertical support moment are affected when a disturbance exists, or when the motion of a limb is modified in an effort to compensate for an existing disturbance. These support reaction forces are normally provided by the limited frictional force, which significantly changes across varying surfaces. Foot sliding can occur if the lateral and longitudinal support force and the vertical support moment exceed the frictional forces of the ground. These unbalanced forces can also lead to instabilities that can cause a fall. So, in some cases, controlling only the ZMP position is not sufficient to maintain the dynamic stability of the robot.

In this thesis, all of the force and moment components of the support foot reaction are controlled, rather than just the position of the ZMP. By addressing

all the support foot forces, not only is the tipping of the robot addressed, but the sliding of the support foot is prevented under bounded disturbances. Since a total of 6 components of the support reaction are controlled, 6 DOFs of the arms of the robot must be used for control. Here, the control inputs are the acceleration of joints, unlike more common approaches in which the positions of joints are used. Additionally, a sliding mode controller is used in the control architecture to increase robustness of the controller. The inputs are taken from the bottom of the support foot, as in the sensor discussed in [30].

CHAPTER 2

APPROACH

In this thesis, a method of control for the swing phase of a humanoid robot's walk in considered. The joint variables of the robot's limbs are denoted as $\mathbf{q}(t)$. Similarly, the desired joint trajectories that constitute a stable walking gait for the humanoid are denoted as $\mathbf{q}^d(t)$. A stable walking gait is one that does not cause the humanoid to tip over, or to enter into an irrecoverable state. As discussed in Chapter Chapter 1, there are two conditions that must be met in order for the walking gait to be considered stable. The first condition states that the position of the ZMP must always be kept within the support polygon. The second condition states that the longitudinal and lateral forces (F_z, F_y) in addition to the vertical twist moment (M_x) of the support foot, cannot exceed the static friction limitation between the foot and ground to prevent slipping. The ZMP equations are

$$\text{ZMP}_y = \frac{M_z}{F_x} \tag{2.1}$$

$$\text{ZMP}_z = \frac{M_y}{F_x}. \tag{2.2}$$

The two conditions for a stable walk can be considered equivalent to maintaining a desired support force vector ($\mathbf{F}_R^d(t)$) and moment vector ($\mathbf{M}_R^d(t)$), where

$$\mathbf{F}_R = [F_x, F_y, F_z]^T,\ \mathbf{M}_R = [M_x, M_y, M_z]^T. \tag{2.3}$$

The desired support force and moment vectors are those that exist in idealistic conditions, that is, when the robot is walking across perfectly level ground with no disturbances throughout the gait. They are calculated based on the joint trajectories of a stable walking gait.

However, a humanoid robot that can walk only in idealistic conditions is not useful outside of a perfect environment. Therefore, it can be assumed that disturbances will exist during its walk, such as uneven terrain or external forces/moments that act directly on the robot's body. These disturbances will affect the support force and moment vectors, deviating from the desired values.

In order to handle these disturbances, it is proposed to design a feedback controller to control the force and moment vectors in real-time to keep them at their desired values, regardless of the existence of disturbances. Specifically, a sliding mode architecture is chosen because of its robust nature in handling disturbances. The control output is defined as

$$\mathbf{y} = \begin{bmatrix} \mathbf{F}_R \\ \mathbf{M}_R \end{bmatrix}, \tag{2.4}$$

with the desired value

$$\mathbf{y}^d(t) = \begin{bmatrix} \mathbf{F}_R^d(t) \\ \\ \mathbf{M}_R^d(t) \end{bmatrix}. \tag{2.5}$$

This thesis will begin by laying out the kinematics of the robot in question, by defining the joint frames and link parameters. Then, the interpolation of the desired values is discussed. The following chapter focuses on the interaction of the forces and moments on the robot, deriving the appropriate angular accelerations of the joints. The disturbance rejection control law is discussed in the next chapter. Finally, the simulation of the robot following the conclusion ends the thesis.

CHAPTER 3

KINEMATICS

The humanoid robot used in this thesis is based off of the BIOLOID Premium Kit Type-A humanoid robot, which has 18 DOF and is displayed in Figure 3.1 and Figure 3.2. This will be modeled using three manipulator chains; a 12-DOF chain from the left foot to the right foot, and two 3-DOF chains from the shoulders to the end of the arms. All of the manipulator chains are comprised of revolute joints. In this chapter, the kinematics of the robot will be considered. Kinematics is the mechanics that describes the motion of a body or system of bodies, without taking forces into account. Specifically for the robot, kinematics will describe how the joints move with respect to each other. This will help in understanding how different joints affect the motion of the robot, and later, how they can be used to reject external disturbances. But before this, a convention needs to be implemented to describe the links connection to each other. The most common convention is the Denavit-Hartenberg (D-H) convention, which is used to assign a coordinate system, or frame, to each link. Next, the frame parameters are defined. Using these frame parameters, the transformation matrices are determined.

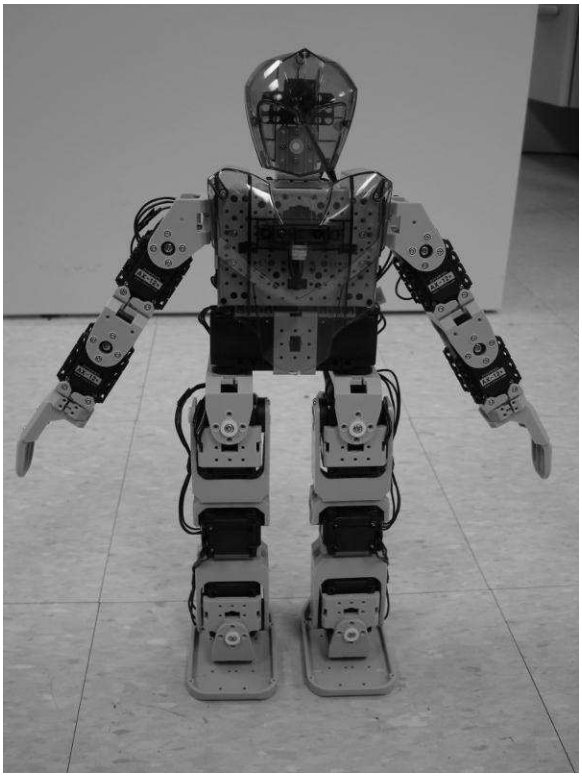

Figure 3.1: BIOLOID Type-A Humanoid Robot in "Zero" Position - Front

Figure 3.2: BIOLOID Type-A Humanoid Robot in "Zero" Position - Angled

3.1 Link Frame Assignment

According to the D-H convention, the frames are attached to the links by following a few rules. As the robot discussed in this thesis is comprised entirely of revolute joints, the discussions will be focused specifically on the conventions associated with revolute joints. Consider two adjacent links, such as those represented in Figure 3.3. Imaginary lines are drawn through the joint axes $i-1$ and i. A common perpendicular is drawn between them. If the axes intersect, then the length of the common perpendicular is zero. The origin of Frame $\{i-1\}$ is assigned to the point of intersection between the joint axis $i-1$ and the common perpendicular. $\hat{Z}_{i-1}$ is

assigned pointing along the joint axis of i. $\hat{X}_{i-1}$ is assigned point along the common perpendicular towards the i joint axis. In the event that the two joint axes intersect, then $\hat{X}_{i-1}$ is assigned to be pointing normal to the plane containing the two joint axes. Finally, $\hat{Y}_{i-1}$ is assigned by completing the right-hand coordinate system. This procedure is repeated for links i, $i+1$,..., $i+N$, where N is the number of links in the system. Additionally, Frame $\{0\}$ is assigned such that it coincides perfectly with Frame $\{1\}$, and Frame $\{N\}$ can be chosen arbitrarily, but usually in a way to cause as many link parameters to become zero. The link parameters are the physical descriptions of the orientation and position relating two links. These link parameters are defined as

Link length a_i is the distance from $\hat{Z}_i$ to $\hat{Z}_{i+1}$, measured along $\hat{X}_i$

Length twist α_i is the angle from $\hat{Z}_i$ to $\hat{Z}_{i+1}$, measured about $\hat{X}_i$

Link offset d_i is the distance from $\hat{X}_i$ to $\hat{X}_{i+1}$, measured along $\hat{Z}_i$

Joint angle θ_i is the angle from $\hat{X}_i$ to $\hat{X}_{i+1}$, measured about $\hat{Z}_i$

The D-H parameters are used to create a matrix representation describing the orientation and position between two link frames, known as a transformation matrix. Each transformation matrix is the result of a series of homogeneous translation and rotation matrices being multiplied together. The result is shown below:

$$ {}^{i-1}_{i}T = \begin{bmatrix} & {}^{i-1}_{i}R & & {}^{i-1}P_{iORG} \\ 0 & 0 & 0 & 1 \end{bmatrix}, \tag{3.1} $$

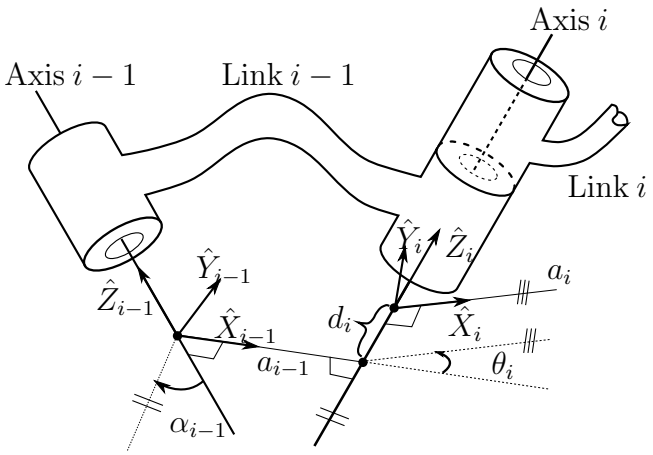

Figure 3.3: Denavit-Hartenberg Frame Assignment and Parameters
(Redrawn based on illustrations in [31])

where ${}^{i-1}_{i}R$ is the 3×3 rotation matrix representing the orientation of frame $\{i\}$ with respect to frame $\{i-1\}$, and ${}^{i-1}P_{iORG}$ is the vector that describes the position of the origin of frame $\{i\}$ with respect to the origin of frame $\{i-1\}$. Note that ${}^{i-1}_{i}T$ is a 4×4 matrix which is multiplied by the 4×1 position vector $P = [P_x, P_y, P_z, 1]^T$ (augmented position vector).

To create the transformation matrix relating the two frames depicted in Figure 3.3, it can be shown that Frame $\{i-1\}$ differs from Frame $\{i\}$ by a series of two rotations and two translations; First a rotation of α_{i-1}, second a translation of a_{i-1}, third a rotation of θ_i, and fourth a translation of d_i. These rotations and translations can be represented by basic homogeneous transformations. For the sake of simplicity, c represents the cosine of an angle, and s represents the sine of an angle (i.e., $c\theta_i$ is the same as $cos(\theta_i)$):

$$\mathrm{Rot}_x(\alpha_{i-1}) = \begin{bmatrix} 1 & 0 & 0 & 0 \\ 0 & c\alpha_{i-1} & -s\alpha_{i-1} & 0 \\ 0 & s\alpha_{i-1} & c\alpha_{i-1} & 0 \\ 0 & 0 & 0 & 1 \end{bmatrix} \tag{3.2}$$

$$\mathrm{Trans}_x(a_{i-1}) = \begin{bmatrix} 1 & 0 & 0 & a_{i-1} \\ 0 & 1 & 0 & 0 \\ 0 & 0 & 1 & 0 \\ 0 & 0 & 0 & 1 \end{bmatrix} \tag{3.3}$$

$$\mathrm{Rot}_z(\theta_i) = \begin{bmatrix} c\theta_i & -s\theta_i & 0 & 0 \\ s\theta_i & c\theta_i & 0 & 0 \\ 0 & 0 & 1 & 0 \\ 0 & 0 & 0 & 1 \end{bmatrix} \tag{3.4}$$

$$\mathrm{Trans}_z(d_i) = \begin{bmatrix} 1 & 0 & 0 & 0 \\ 0 & 1 & 0 & 0 \\ 0 & 0 & 1 & d_i \\ 0 & 0 & 0 & 1 \end{bmatrix}. \tag{3.5}$$

These matrices are multiplied together in their respective order:

$$^{i-1}_{i}T = \mathrm{Rot}_x(\alpha_{i-1})\mathrm{Trans}_x(a_{i-1})\mathrm{Rot}_z(\theta_i)\mathrm{Trans}_z(d_i). \tag{3.6}$$

And the result is the transformation matrix that relates the position and orientation of two adjacent frames:

$$ {}^{i-1}_{i}T = \begin{bmatrix} c\theta_i & -s\theta_i & 0 & a_{i-1} \\ s\theta_i c\alpha_{i-1} & c\theta_i c\alpha_{i-1} & -s\alpha_{i-1} & -s\alpha_{i-1}d_i \\ s\theta_i s\alpha_{i-1} & c\theta_i s\alpha_{i-1} & c\alpha_{i-1} & c\alpha_{i-1}d_i \\ 0 & 0 & 0 & 1 \end{bmatrix}. \tag{3.7} $$

These link transformations can be used to relate a link frame $\{N\}$ with the base frame $\{0\}$:

$$ {}^{0}_{N}T = {}^{0}_{1}T\,{}^{1}_{2}T\,{}^{2}_{3}T \ldots {}^{N-1}_{N}T, \tag{3.8} $$

where ${}^{0}_{N}T$ is a function of all n joint variables. Using this, the frame assignments for the robot are shown in Figure 3.4.

3.2 Link Parameters of the BIOLOID Type-A Humanoid

After the frame assignments are made, the link parameters are extracted from the geometry of the robot, as mentioned in Section 3.1. These parameters are used with Equation (3.7) to form the numerical value of the transformation matrix for any given joint angle θ_i. The numerical values of the link parameters are shown in Table 3.1 and Table 3.2.

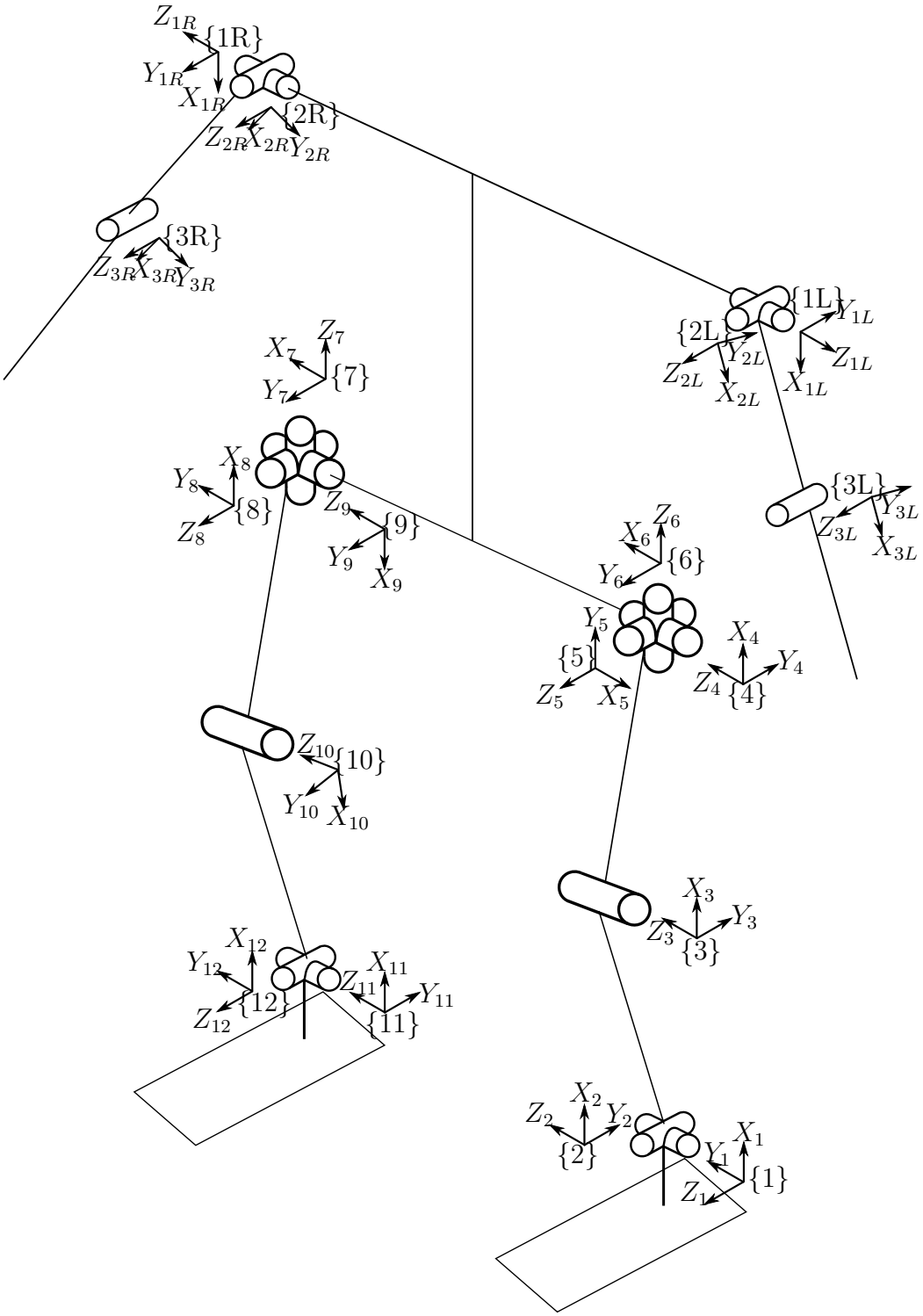

Figure 3.4: Frame Assignments

Table 3.1: Link Parameters for Legs (angles in radians, length in millimeters)

Link i	α_{i-1}	a_{i-1}	d_i	θ_i
1	0	0	0	θ_1
2	$-\pi/2$	0	0	θ_2
3	0	77.494	0	θ_3
4	0	77.978	0	θ_4
5	$\pi/2$	0	0	θ_5
6	$-\pi/2$	0	0	θ_6
7	0	76.987	0	θ_7
8	$-\pi/2$	0	0	θ_8
9	$-\pi/2$	0	0	θ_9
10	0	77.978	0	θ_{10}
11	0	77.494	0	θ_{11}
12	$\pi/2$	0	0	θ_{12}

Table 3.2: Link Parameters for Left and Right Arms (angles in radians, length in millimeters)

Link i	α_{i-1}	a_{i-1}	d_i	θ_i
L1	0	0	0	θ_{1L}
L2	$\pi/2$	14.503	0	θ_{2L}
L3	0	67.488	0	θ_{3L}
R1	0	0	0	θ_{1R}
R2	$3\pi/2$	14.503	0	θ_{2R}
R3	0	67.488	0	θ_{3R}

3.3 Relating the Arm Chains to the Leg Chain

As previously mentioned, there are three manipulator chains modeled for the humanoid. In order to relate the joint frames of the arms to the base frame of the legs, there has to be a transformation matrix describing the position and orientation of the base frames of the arms, to some link on the legs. It is logical to assume that the best choice is to relate the shoulders to the body, as these are the physical connections between the leg chain and arm chains. The body is part of Link 6 in

the leg chain, and the shoulders are the base frames of the arm chains, with the left shoulder being part of Link 1L and the right shoulder being part of Link 1R. The transformation matrix is formed by assuming the body frame (Frame {6}) is the base frame of the shoulders and, unlike normal D-H convention, does not coincide with the first frames of the arms (Frame $\{1L\}$ and Frame $\{1R\}$). The numerical transformation matrices describing the shoulders to the body are shown below, where the lengths are in millimeters.

$$ {}^{6}_{1L}T = \begin{bmatrix} 0 & 0 & -1 & -33.520 \\ 0 & -1 & 0 & -0.002 \\ -1 & 0 & 0 & 121.250 \\ 0 & 0 & 0 & 1 \end{bmatrix} \tag{3.9} $$

$$ {}^{6}_{1R}T = \begin{bmatrix} 0 & 0 & 1 & 110.100 \\ 0 & 1 & 0 & -0.002 \\ -1 & 0 & 0 & 121.520 \\ 0 & 0 & 0 & 1 \end{bmatrix} \tag{3.10} $$

These transformation matrices and frame assignments are crucial for defining the motion of the robot. They coordinate the motion of the robot in a logical way so that it can perform the appropriate motion and, as will be shown later, be able to determine what accelerations are needed to compensate for disturbances. Prior to acceleration, however, the position and velocity of the joints need to be defined such that it gives a smooth walking motion.

CHAPTER 4

GAIT

Gait is the pattern of movement of an animal's limbs, such as what is seen in walking, jogging, running, or galloping. In humans, these gaits are, in general, walking jogging, and running, with each gait used in different situations, typically based on speed and terrain. Humans most often use the walking gait in day-to-day life, as it consumes little energy relative to the other gaits. Additionally, modern environments such as buildings and cities, do not facilitate the higher speed gaits as these are less maneuverable. It is this environment that would account for the majority of the terrains and conditions a humanoid robot would encounter. It is, therefore important to focus on the walking gait of a humanoid robot.

4.1 Conversion Factors of Gait Values

The gait of the robot in this thesis is taken from the walking gait that is one of the pre-programmed gaits included in the BIOLOID Premium Kit software, with some modifications to the arm positions. The values of the gait provided by the software are given in terms of step position of the Dynamixel AX-12 servos, which drive the joints of the robot. As can be seen in Figure 4.1, the angular position of

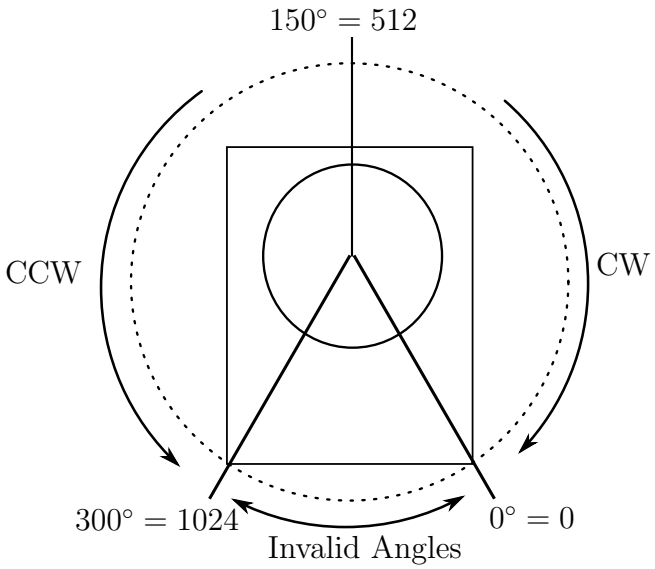

Figure 4.1: Representation of the Dynamixel AX-12 Servo Range
Taken from User Manual [32]

the servo's horn corresponds to a value of 0 to 1024, representing the angles 0° to 300°, respectively. This is due to the programming and digital nature of the servo. As such, the servo's horn can only rotate in approximately 0.293° increments.

Using the steps of the motor is itself not particularly helpful when it comes to determining the velocity and acceleration of a joint. Additionally, the servo step positions are dependent on the orientation of the servo motors themselves, rather than the joint. This is an unnecessary complication when trying to formulate the kinematics of the robot, which is best done with the joint angles themselves measured in degrees. Therefore a conversion factor must be made between servo step positions and joint angle in degrees. This is especially true as the value for the zero servomotor position on the individual servos does not correlate well to what is considered the "zero position" of the humanoid joints, that is, the position where the joint angles

are defined as zero degrees when defining link frame transformations. This position is shown in Chapter 3 in Figure 3.1 and Figure 3.2. The conversion factors are linear conversions that takes into account the offset between the zero servomotor position on the servo, and zero degrees for the joint angles. It then converts the step position to degrees. This quantity is then multiplied by the conversion factor relating the number of degrees per servomotor step position, which, as stated previously, is approximately 0.293° per step position. These conversion factors are shown below where q_i and q_{bi} represent the converted value and servo step position, respectively. q_1 through q_12 represent the joint angles of the leg joints, q_{1L} through q_{3L} represent the joint angles of the left arm, andq_{1R} through q_{3R} represent the joint angles of the right arm, as shown in Figure Figure 3.4:

For the Leg/Body Chain:

$$q_1 = (-512 + q_{b1}) \cdot 0.293 \frac{\text{degrees}}{\text{step}} \tag{4.1}$$

$$q_2 = (-474.453 + q_{b2}) \cdot 0.293 \frac{\text{degrees}}{\text{step}} \tag{4.2}$$

$$q_3 = (-587.093 + q_{b3}) \cdot 0.293 \frac{\text{degrees}}{\text{step}} \tag{4.3}$$

$$q_4 = (549.547 - q_{b4}) \cdot 0.293 \frac{\text{degrees}}{\text{step}} \tag{4.4}$$

$$q_5 = (204.8 - q_{b5}) \cdot 0.293 \frac{\text{degrees}}{\text{step}} \tag{4.5}$$

$$q_6 = (-51.6 + q_{b6}) \cdot 0.293 \frac{\text{degrees}}{\text{step}} \tag{4.6}$$

$$q_7 = (358 - q_{b7}) \cdot 0.293 \frac{\text{degrees}}{\text{step}} \tag{4.7}$$

$$q_8 = (-819.2 + q_{b8}) \cdot 0.293 \frac{\text{degrees}}{\text{step}} \tag{4.8}$$

$$q_9 = (1088.853 - q_{b9}) \cdot 0.293 \frac{\text{degrees}}{\text{step}} \tag{4.9}$$

$$q_{10} = (-436.907 + q_{b10}) \cdot 0.293 \frac{\text{degrees}}{\text{step}} \tag{4.10}$$

$$q_{11} = (64.853 + q_{b11}) \cdot 0.293 \frac{\text{degrees}}{\text{step}} \tag{4.11}$$

$$q_{12} = (512 - q_{b12}) \cdot 0.293 \frac{\text{degrees}}{\text{step}} \tag{4.12}$$

For the Left Arm Chain:

$$q_{1L} = (-818 + q_{b1L}) \cdot 0.293 \frac{\text{degrees}}{\text{step}} \tag{4.13}$$

$$q_{2L} = (-819.429 + q_{b2L}) \cdot 0.293 \frac{\text{degrees}}{\text{step}} \tag{4.14}$$

$$q_{3L} = (-512 + q_{b3L}) \cdot 0.293 \frac{\text{degrees}}{\text{step}} \tag{4.15}$$

For the Right Arm Chain:

$$q_{1R} = (-205 + q_{b1R}) \cdot 0.293 \frac{\text{degrees}}{\text{step}} \tag{4.16}$$

$$q_{2R} = (-437.429 + q_{b2R}) \cdot 0.293 \frac{\text{degrees}}{\text{step}} \tag{4.17}$$

$$q_{3R} = (-512 + q_{b3R}) \cdot 0.293 \frac{\text{degrees}}{\text{step}} \tag{4.18}$$

The converted values are displayed in Table 4.1, Table 4.2, Table 4.3, and Table 4.4.

4.2 Polynomial Fit

Now that the servo step positions have been converted to joint angles in degrees, a smooth function can be determined by fitting a polynomial to the data. The coefficients are determined by using the MATLAB function *polyfit*, which uses a least squares polynomial to fit the data in accordance with the degree specified. Here, fifth-order polynomials are used. An error analysis is done to ensure that the original

Table 4.1: Robot's Leg/Body Joint Angles at the Start and End of a Step in Degrees (First Half-Period)

Time (s)	0	0.08	0.16	0.24	0.32	0.40	0.48
q_1	4.688	2.637	0.586	-1.465	-2.930	-3.809	-4.395
q_2	-11.266	-14.488	-16.539	-18.297	-19.469	-20.641	-21.520
q_3	40.988	43.039	44.211	44.797	44.797	44.797	44.797
q_4	-48.180	-47.594	-46.422	-45.250	-44.078	-42.906	-42.027
q_5	-94.688	-92.637	-91.172	-91.758	-92.930	-94.688	-95.566
q_6	181.172	181.172	181.172	181.172	181.172	181.172	181.172
q_7	1.172	1.172	1.172	1.172	1.172	1.172	1.172
q_8	-97.031	-99.082	-101.426	-104.356	-107.578	-110.508	-113.428
q_9	206.793	202.691	201.227	204.449	212.066	222.027	234.332
q_{10}	-37.473	-33.078	-32.199	-38.938	-50.656	-64.133	-78.195
q_{11}	209.723	209.430	210.016	213.238	217.340	220.856	222.613
q_{12}	7.031	9.082	11.133	13.184	15.527	17.578	19.922

Table 4.2: Robot's Leg/Body Joint Angles at the Start and End of a Step in Degrees (Second Half-Period)

Time (s)	0.56	0.64	0.72	0.80	0.88	0.96	1.04
q_1	-4.395	-3.809	-2.930	-1.465	0.586	2.637	4.688
q_2	-22.984	-23.863	-25.035	-26.207	-27.379	-28.551	-29.137
q_3	44.797	44.797	44.797	44.797	44.211	43.039	40.988
q_4	-40.563	-39.684	-38.512	-37.340	-35.582	-33.531	-30.309
q_5	-95.566	-94.688	-92.930	-91.758	-91.172	-92.637	-94.688
q_6	181.172	181.172	181.172	181.172	181.172	181.172	181.172
q_7	1.172	1.172	1.172	1.172	1.172	1.172	1.172
q_8	-113.438	-110.508	-107.578	-104.356	-101.426	-99.082	-97.031
q_9	241.656	239.898	236.383	232.281	229.059	228.473	228.766
q_{10}	-78.195	-64.133	-50.656	-38.938	-32.199	-33.078	-37.766
q_{11}	215.289	202.984	193.023	185.406	182.184	183.648	187.750
q_{12}	19.922	17.578	15.527	13.184	11.133	9.082	7.031

Table 4.3: Robot's Arm Joint Angles at the Start and End of a Step in Degrees (First Half-Period)

Time (s)	0	0.08	0.16	0.24	0.32	0.40	0.48
q_{1L}	8.789	8.789	7.910	6.452	3.516	0.586	-2.930
q_{2L}	-27.665	-27.665	-27.665	-27.665	-27.665	-27.665	-27.665
q_{3L}	2.930	2.930	3.516	4.688	6.445	8.496	10.840
q_{1R}	26.367	26.367	27.246	29.004	31.641	34.570	38.086
q_{2R}	-40.555	-40.555	-40.555	-40.555	-40.555	-40.555	-40.555
q_{3R}	-26.367	-26.367	-26.953	-28.125	-29.883	-31.934	-34.277

Table 4.4: Robot's Arm Joint Angles at the Start and End of a Step in Degrees (Second Half-Period)

Time (s)	0.56	0.64	0.72	0.80	0.88	0.96	1.04
q_{1L}	-6.738	-10.840	-14.648	-18.164	-21.094	-23.731	-25.488
q_{2L}	-27.665	-27.665	-27.665	-27.665	-27.665	-27.665	-27.665
q_{3L}	13.477	15.820	18.457	20.801	22.852	24.609	25.781
q_{1R}	41.895	45.996	49.805	53.320	56.250	58.887	60.645
q_{2R}	-40.555	-40.555	-40.555	-40.555	-40.555	-40.555	-40.555
q_{3R}	-36.914	-39.258	-41.895	-44.238	-46.289	-48.047	-49.219

steps and the fitted curves are sufficiently close. Note that the data represents the original steps that are pre-programmed in the BIOLOID demo software, and they are arbitrary. They are used as a reference for the simplicity of choosing a gait. So, the difference between the curve fits and the original steps (data) have no effect on the results of this research.

Just for a reference, a comparison of the data with the polynomial fit for all of the joint angles is shown in Figure 4.2 - Figure 4.5 for the legs and body, and Figure 4.6 and Figure 4.7 for the arms. Additionally, the percent error between the data points

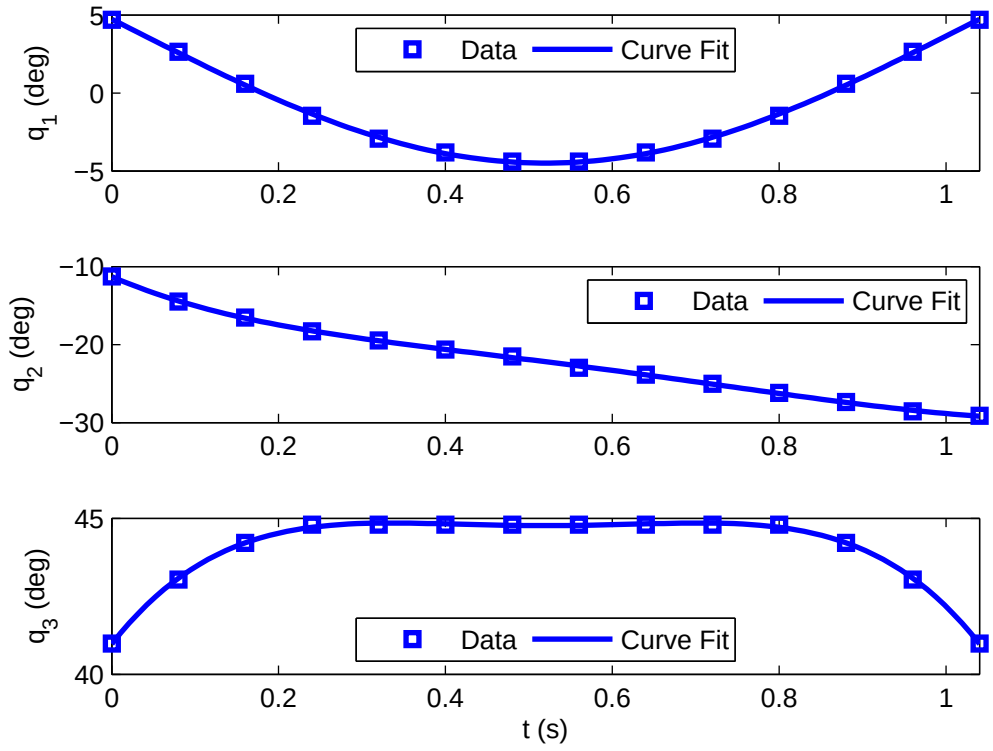

Figure 4.2: Leg/Body Joints 1-3 Polynomial Fit Comparison

and the corresponding values on the polynomial fit are listed in Table 4.5 and Table 4.6 for the legs and body, and Table 4.7 and Table 4.8 for the arms.

The position, velocity, and acceleration equations are

$$q_i(t) = A_i t^5 + B_i t^4 + C_i t^3 + D_i t^2 + E_i t + F_i \tag{4.19}$$

$$\dot{q}_i(t) = 5A_i t^4 + 4B_i t^3 + 3C_i t^2 + 2D_i t + E_i \tag{4.20}$$

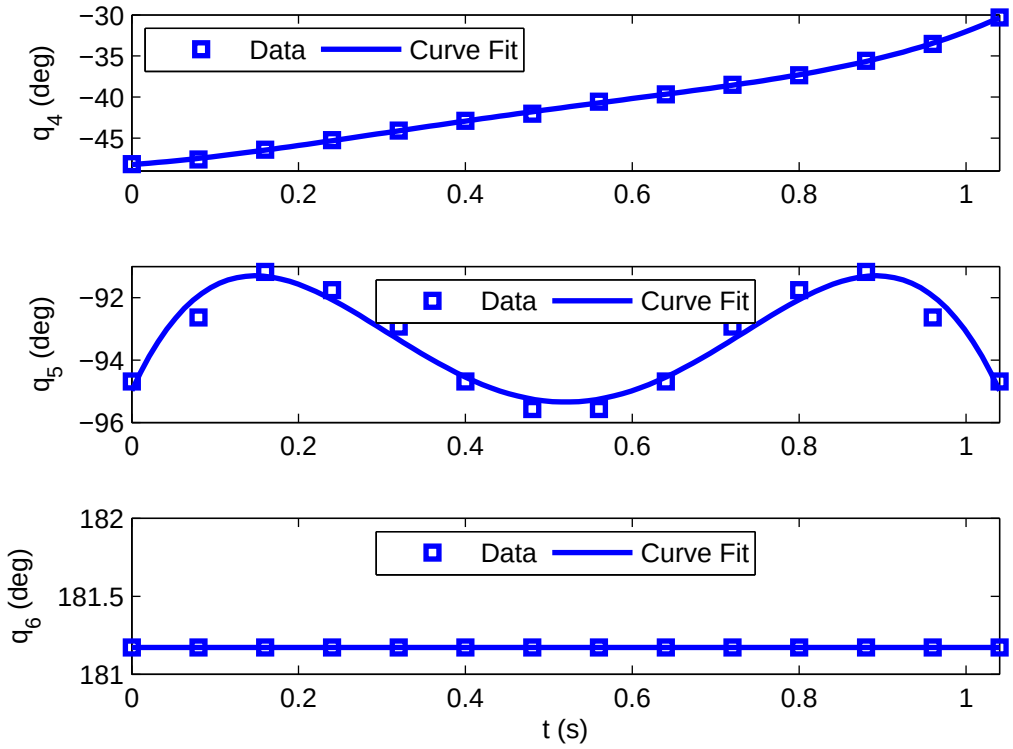

Figure 4.3: Leg/Body Joints 4-6 Polynomial Fit Comparison

Table 4.5: Error of the Polynomial Fit - Legs/Body (First Half-Period)

	Percent Error						
Time (s)	0	0.08	0.16	0.24	0.32	0.40	0.48
q_1	0.788	2.219	14.060	8.288	3.132	2.040	0.717
q_2	0.266	0.590	0.474	0.295	0.248	0.109	0.701
q_3	0.042	0.100	0.011	0.188	0.111	0.056	0.047
q_4	0.099	0.263	0.090	0.147	0.086	0.051	0.561
q_5	0.306	0.750	0.157	0.329	0.447	0.148	0.329
q_6	0.000	0.000	0.000	0.000	0.000	0.000	0.000
q_7	0.000	0.000	0.000	0.000	0.000	0.000	0.000
q_8	0.369	0.716	0.210	0.433	0.648	0.405	0.910
q_9	0.518	1.013	0.356	0.604	0.947	0.676	0.976
q_{10}	6.386	14.882	3.115	7.922	8.670	3.030	7.540
q_{11}	0.645	1.388	0.184	0.927	1.122	0.196	1.646
q_{12}	3.974	5.769	2.259	3.008	3.652	2.422	4.484

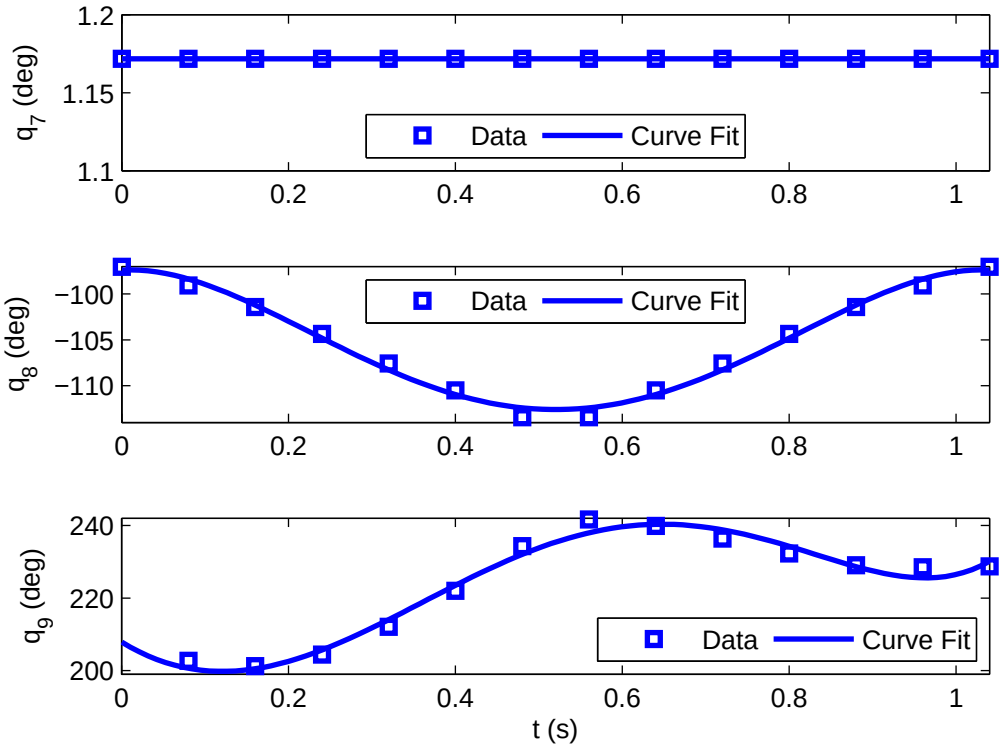

Figure 4.4: Leg/Body Joints 7-9 Polynomial Fit Comparison

Table 4.6: Error of the Polynomial Fit - Legs/Body (Second Half-Period)

	Percent Error						
Time (s)	0.56	0.64	0.72	0.80	0.88	0.96	1.04
q_1	0.717	2.040	3.132	8.288	14.060	2.219	0.788
q_2	1.025	0.092	0.151	0.254	0.152	0.439	0.163
q_3	0.047	0.056	0.111	0.188	0.011	0.100	0.042
q_4	0.372	0.057	0.125	0.145	0.220	0.255	0.099
q_5	0.329	0.148	0.447	0.329	0.157	0.750	0.306
q_6	0.000	0.000	0.000	0.000	0.000	0.000	0.000
q_7	0.000	0.000	0.000	0.000	0.000	0.000	0.000
q_8	0.910	0.405	0.648	0.433	0.210	0.716	0.369
q_9	1.516	0.180	1.032	0.851	0.169	1.273	0.591
q_{10}	7.529	3.060	8.689	7.881	3.203	14.777	6.310
q_{11}	1.063	0.739	1.040	0.666	0.393	1.118	0.571
q_{12}	4.484	2.422	3.652	3.008	2.259	5.769	3.974

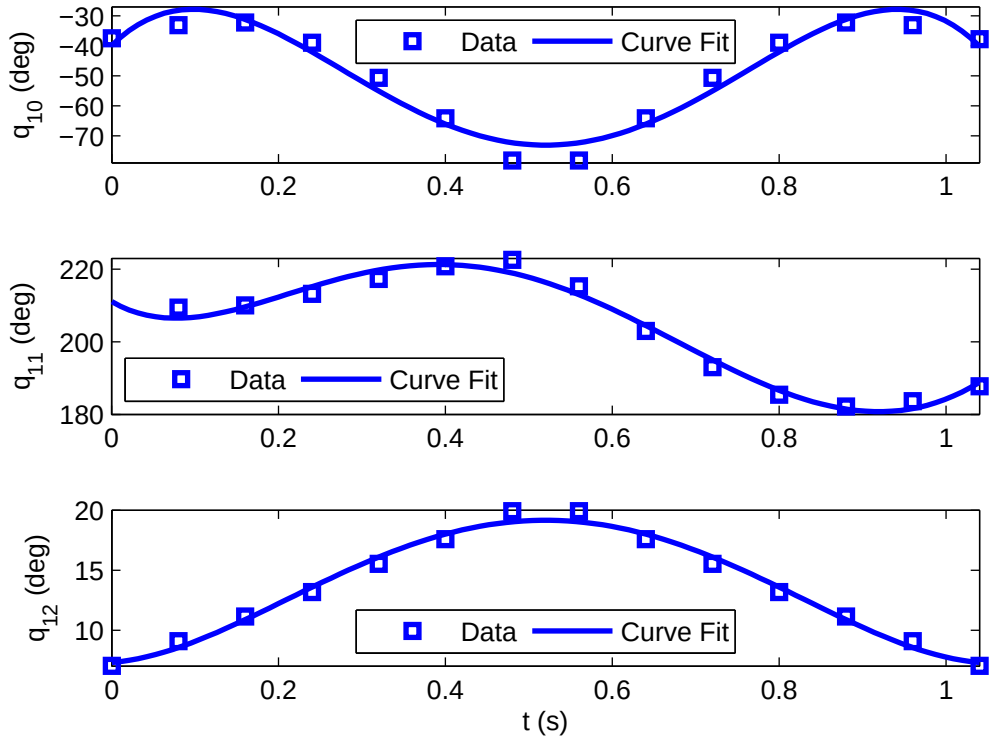

Figure 4.5: Leg/Body Joints 10-12 Polynomial Fit Comparison

Table 4.7: Error of the Polynomial Fit - Arms (First Half-Period)

	Percent Error						
Time (s)	0	0.08	0.16	0.24	0.32	0.40	0.48
q_{1L}	0.171	0.187	0.480	0.221	4.073	4.411	2.355
q_{2L}	0.000	0.000	0.000	0.000	0.000	0.000	0.000
q_{3L}	0.582	1.407	0.059	0.967	0.230	0.112	0.111
q_{1R}	0.057	0.062	0.139	0.047	0.453	0.075	0.181
q_{2R}	0.000	0.000	0.000	0.000	0.000	0.000	0.000
q_{3R}	0.065	0.156	0.008	0.161	0.050	0.030	0.035

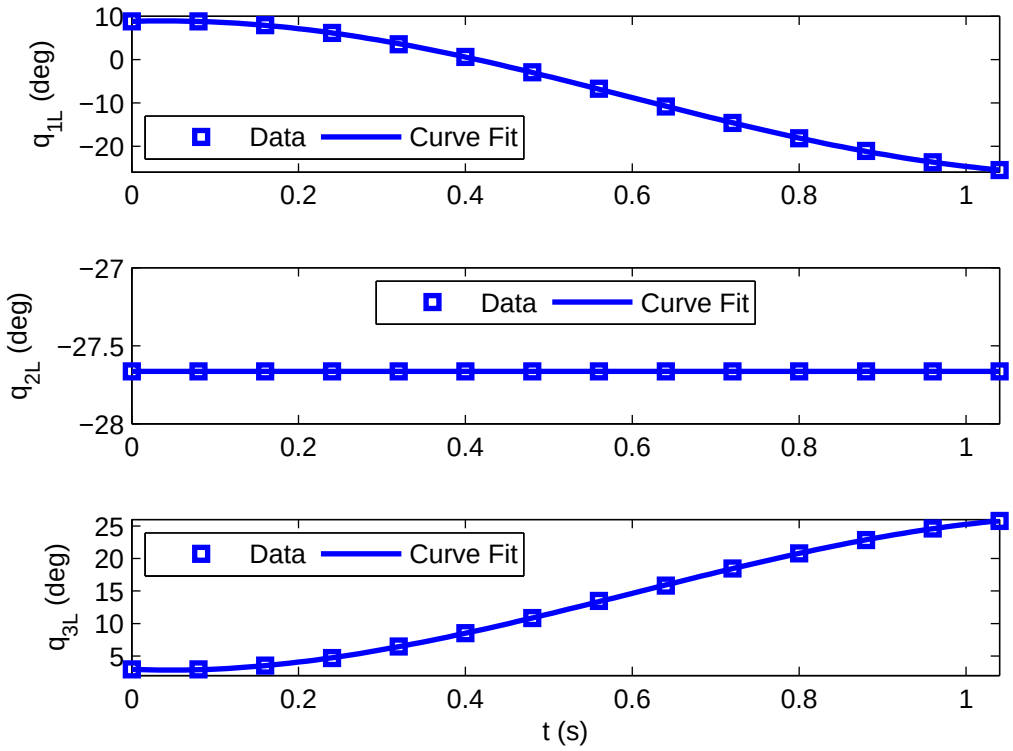

Figure 4.6: Left Arm Joints Polynomial Fit Comparison

Table 4.8: Error of the Polynomial Fit - Arms (Second Half-Period)

	Percent Error						
Time (s)	0.56	0.64	0.72	0.80	0.88	0.96	1.04
q_{1L}	1.473	0.699	0.408	0.222	0.524	0.162	0.004
q_{2L}	0.000	0.000	0.000	0.000	0.000	0.000	0.000
q_{3L}	0.851	0.679	0.088	0.041	0.097	0.133	0.049
q_{1R}	0.237	0.163	0.120	0.076	0.196	0.065	0.002
q_{2R}	0.000	0.000	0.000	0.000	0.000	0.000	0.000
q_{3R}	0.311	0.274	0.039	0.019	0.048	0.068	0.025

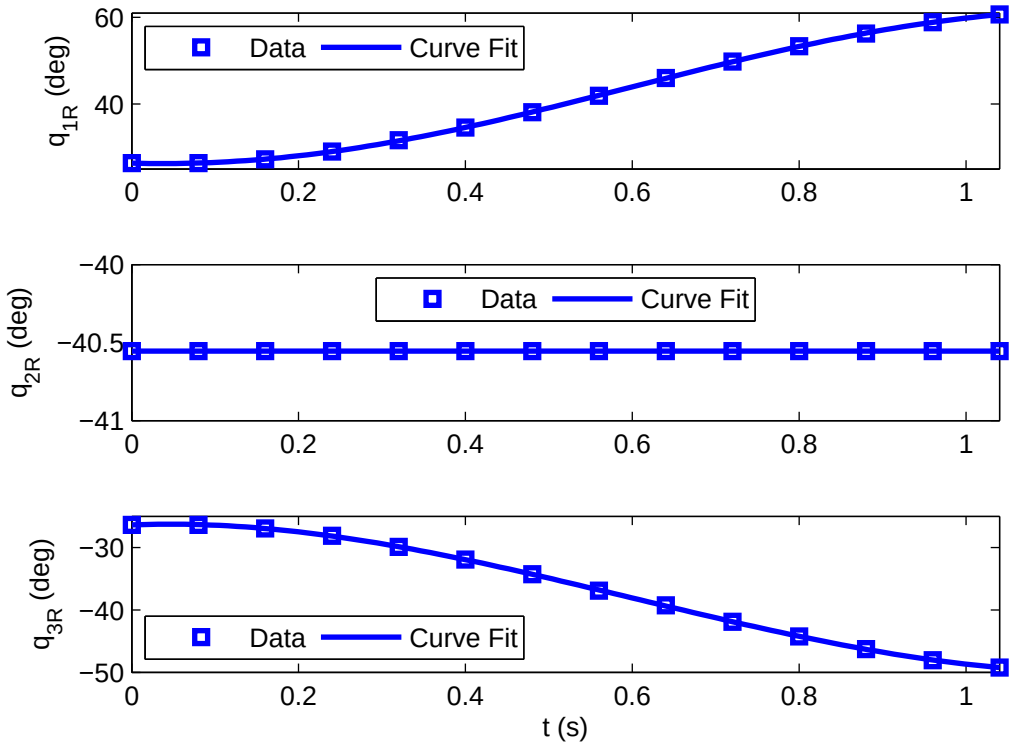

Figure 4.7: Right Arm Joints Polynomial Fit Comparison

$$\ddot{q}_i(t) = 20A_i t^3 + 12B_i t^2 + 6C_i t + 2D_i, \tag{4.21}$$

where A_i, B_i, C_i, D_i, E_i, F_i are the coefficients of the polynomial for the ith joint, including the arm joints. These joint angles are the desired joint angles, velocities, and accelerations for the humanoid, and will be vital in the control of the humanoid and stabilization against external disturbances. But first, the input-output model of the robot must be defined.

CHAPTER 5

INPUT-OUTPUT MODEL

The input-output (I/O) model describes the interaction of the forces and moments on the robot. It serves as the basis on which the control is implemented. The equations are solved for the output variables in terms of the input variables. In the case of the robot, the reaction force and moment the robot's foot exerts on the ground, $\mathbf{F}_R$ and $\mathbf{M}_R$, are the output variables. The accelerations of the arm joints, $\ddot{\mathbf{q}}_a$, are the input variables. The force and moments are represented on the robot as a system of rigid bodies that are in a state of dynamic balance at time t. The free body diagram (FBD) and the kinetic diagram (KD) are shown below in Figure 5.1. $\mathbf{F}_s$ and $\mathbf{M}_s$ are the support force and moment the ground imparts to the robot's foot, respectively. The variables m_i and $\mathbf{I}_i^B$ are the mass and centroidal moment of inertia matrices defined in local frame B for link i of the robot, respectively. $\boldsymbol{\omega}_i^B$ is the angular velocity of link i in its local frame. $\mathbf{r}_i$ is the global position vector of the centroid of link i. $\mathbf{R}_{0i}$ is the rotation matrix that converts the local frame of link i to the base inertial frame 0, specifically the base of the robot's left foot. It is important to note that $\mathbf{R}_{0i}$ is a function of θ_1, θ_2,..., θ_i. By equating the external forces and moments as

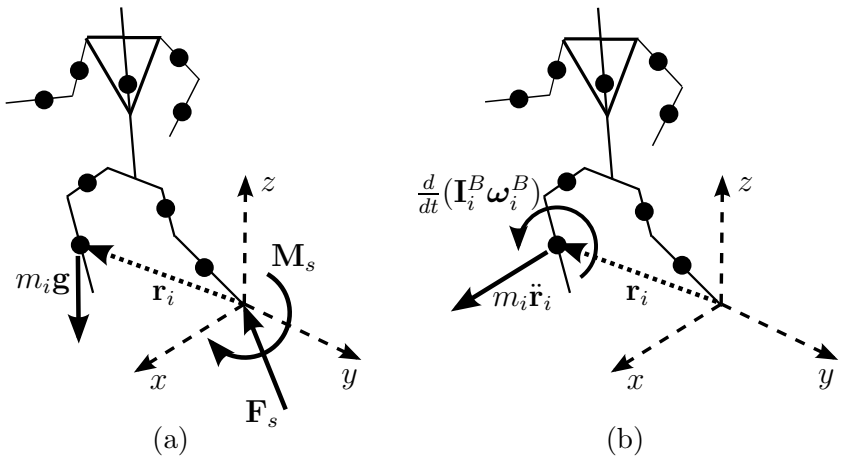

Figure 5.1: a) Free Body Diagram, b) Kinematic Diagram

shown in Figure 5.1(a) with the inertial forces and moments shown in Figure 5.1(b), Newton's second law, as applied to the robot shown, is

$$\mathbf{F}_s + \sum m_i\mathbf{g} = \sum m_i\ddot{\mathbf{r}}_i, \tag{5.1}$$

$$\mathbf{M}_s + \sum \mathbf{r}_i \times m_i\mathbf{g} = \sum(\mathbf{R}_{0i}\tfrac{d}{dt}(\mathbf{I}_i^B\boldsymbol{\omega}_i^B) + \mathbf{r}_i \times m_i\ddot{\mathbf{r}}_i). \tag{5.2}$$

The support force and moment are equal and opposite to the reaction force and moment. From this, the reaction force and moment can replace the support force and moment in Equation (5.1) and Equation (5.2). Isolating $\mathbf{F}_R$ and $\mathbf{M}_R$ gives

$$\mathbf{F}_R = \sum(m_i\mathbf{g} - m_i\ddot{\mathbf{r}}_i), \tag{5.3}$$

$$\mathbf{M}_R = \sum(\mathbf{r}_i \times m_i\mathbf{g} - \mathbf{R}_{0i}(\mathbf{I}_i^B\dot{\boldsymbol{\omega}}_i^B + \boldsymbol{\omega}_i^B \times \mathbf{I}_i^B\boldsymbol{\omega}_i^B) - \mathbf{r}_i \times m_i\ddot{\mathbf{r}}_i). \tag{5.4}$$

The linear velocity of the center of mass of link i as expressed in the inertial frame ($\dot{\mathbf{r}}_i$) is derived in terms of the joint rate vector using Jacobian matrices.

$$\dot{\mathbf{r}}_i = \begin{bmatrix} \mathbf{J}_{ai} & \mathbf{J}_{bi} \end{bmatrix} \begin{bmatrix} \dot{\mathbf{q}}_a \\ \\ \dot{\mathbf{q}}_b \end{bmatrix} \quad i = 1, ..., n \tag{5.5}$$

Here, $\dot{\mathbf{q}}_a$ is a 6×1 vector of the joint rates of the arm with $\mathbf{J}_{ai}$ being the respective Jacobian matrix with size 3×6. This Jacobian matrix is defined as

$$\mathbf{J}_{ai} = \frac{\partial \dot{\mathbf{r}}_i}{\partial \dot{\mathbf{q}}_a^T} = \begin{bmatrix} \frac{\partial \dot{r}_{i1}}{\partial \dot{q}_{a1}} & \frac{\partial \dot{r}_{i1}}{\partial \dot{q}_{a2}} & \dots & \frac{\partial \dot{r}_{i1}}{\partial \dot{q}_{aN}} \\ \frac{\partial \dot{r}_{i2}}{\partial \dot{q}_{a1}} & \frac{\partial \dot{r}_{i2}}{\partial \dot{q}_{a2}} & \dots & \frac{\partial \dot{r}_{i2}}{\partial \dot{q}_{aN}} \\ \frac{\partial \dot{r}_{i3}}{\partial \dot{q}_{a1}} & \frac{\partial \dot{r}_{i3}}{\partial \dot{q}_{a2}} & \dots & \frac{\partial \dot{r}_{i3}}{\partial \dot{q}_{aN}} \end{bmatrix}. \tag{5.6}$$

Similarly, $\dot{\mathbf{q}}_b$ is a 12×1 vector of the joint rates of the body with $\mathbf{J}_{bi}$ being the respective Jacobian matrix with size 3×12 and defined in a similar manner to $\mathbf{J}_{ai}$. The relation for the angular velocity of the robot's links as expressed in the inertial frame $\boldsymbol{\omega}_i$ can be written as

$$\boldsymbol{\omega}_i = \begin{bmatrix} \mathbf{G}_{ai} & \mathbf{G}_{bi} \end{bmatrix} \begin{bmatrix} \dot{\mathbf{q}}_a \\ \\ \dot{\mathbf{q}}_b \end{bmatrix} \quad i = 1, ..., n, \tag{5.7}$$

where $\mathbf{G}_{ai}$ and $\mathbf{G}_{bi}$ are the same size as $\mathbf{J}_{ai}$ and $\mathbf{J}_{bi}$, respectively. They are also defined in a similar manner:

$$\mathbf{G}_{ai} = \frac{\partial \omega_i}{\partial \dot{\mathbf{q}}_a{}^T} = \begin{bmatrix} \frac{\partial \omega_{i1}}{\partial \dot{q}_{a1}} & \frac{\partial \omega_{i1}}{\partial \dot{q}_{a2}} & \cdots & \frac{\partial \omega_{i1}}{\partial \dot{q}_{aN}} \\ \frac{\partial \omega_{i2}}{\partial \dot{q}_{a1}} & \frac{\partial \omega_{i2}}{\partial \dot{q}_{a2}} & \cdots & \frac{\partial \omega_{i2}}{\partial \dot{q}_{aN}} \\ \frac{\partial \omega_{i3}}{\partial \dot{q}_{a1}} & \frac{\partial \omega_{i3}}{\partial \dot{q}_{a2}} & \cdots & \frac{\partial \omega_{i3}}{\partial \dot{q}_{aN}} \end{bmatrix}. \tag{5.8}$$

By taking the derivatives of the linear and angular velocities in Equation (5.5) and Equation (5.7), the respective accelerations are found.

$$\begin{aligned} \ddot{\mathbf{r}}_i &= \mathbf{J}_{ai}\ddot{\mathbf{q}}_a + (\dot{\mathbf{J}}_{ai}\dot{\mathbf{q}}_a + \mathbf{J}_{bi}\ddot{\mathbf{q}}_b + \dot{\mathbf{J}}_{bi}\dot{\mathbf{q}}_b) \\ &= \mathbf{J}_{ai}\ddot{\mathbf{q}}_a + \mathbf{f}_{ti} \end{aligned} \tag{5.9}$$

$$\begin{aligned} \dot{\boldsymbol{\omega}}_i &= \mathbf{G}_{ai}\ddot{\mathbf{q}}_a + (\dot{\mathbf{G}}_{ai}\dot{\mathbf{q}}_a + \mathbf{G}_{bi}\ddot{\mathbf{q}}_b + \dot{\mathbf{G}}_{bi}\dot{\mathbf{q}}_b) \\ &= \mathbf{G}_{ai}\ddot{\mathbf{q}}_a + \mathbf{f}_{ri} \end{aligned} \tag{5.10}$$

By substituting the accelerations into the force and moment equations from Equation (5.3) and Equation (5.4), and rearranging the terms to isolate the joint accelerations of the arms, it can be shown

$$\begin{aligned} \mathbf{F}_R &= (-\sum m_i \mathbf{J}_{ai})\ddot{\mathbf{q}}_a + (\sum m_i(\mathbf{g} - \mathbf{f}_{ti})) \\ &= \mathbf{b}_f\ddot{\mathbf{q}}_a + \mathbf{f}_f \end{aligned} \tag{5.11}$$

$$
\begin{aligned}
\mathbf{M}_R &= [-\sum(\mathbf{R}_{0i}\mathbf{I}_i^B\mathbf{G}_{ai} + m_i\mathbf{r}_i \times \mathbf{J}_{ai})]\ddot{\mathbf{q}}_a \\
&+ [\sum(m_i\mathbf{r}_i \times \mathbf{g} - \mathbf{R}_{0i}(\boldsymbol{\omega}_i^B \times \mathbf{I}_i^B\boldsymbol{\omega}_i^B + \mathbf{I}_i^B\mathbf{f}_{ri}) - m_i\mathbf{r}_i \times \mathbf{f}_{ti}] \\
&= \mathbf{b}_m\ddot{\mathbf{q}}_a + \mathbf{f}_m. \qquad (5.12)
\end{aligned}
$$

These force and moment equations can now be combined as a system of equations that completes the input-output model of the robot.

$$
\begin{aligned}
\begin{bmatrix} \mathbf{F}_R \\ \mathbf{M}_R \end{bmatrix} &= \begin{bmatrix} \mathbf{b}_f \\ \mathbf{b}_m \end{bmatrix} \ddot{\mathbf{q}}_a + \begin{bmatrix} \mathbf{f}_f \\ \mathbf{f}_m \end{bmatrix} \\
\mathbf{y} &= \mathbf{b}\ddot{\mathbf{q}}_a + \mathbf{f} \qquad (5.13)
\end{aligned}
$$

The input-output model is now completed, with the acceleration of the arm joints, $\ddot{\mathbf{q}}_a$, as the input variable, and the reaction force and moment, $\mathbf{F}_R$ and $\mathbf{M}_R$, as the output variable, collectively denoted by $\mathbf{y}$. With the dynamics of the robot fully realized, the controller can be designed to allow the robot to compensate for disturbances during its gait by controlling the accelerations of the arm joints.

CHAPTER 6

CONTROLLER

In order for the humanoid robot to handle disturbances during its walking gait, it is crucial for the robot to implement a robust controller that can quickly, and accurately carry out this duty. Without a controller, the robot could only perform in an ideal environment where it could execute its desired task without concern for any disturbances. In a real world environment, this is not useful, as a humanoid robot will need to compensate for changes in terrain and external disturbances. Compensating for a disturbance consists of two parts; the robot must react to reject the disturbance and then recover its motion by returning to the desired gait. The method of rejecting the disturbance is shown in Section 6.1, and then the method of resuming the desired gait is shown in Section 6.2.

6.1 Disturbance Rejection

For the robot in question, the inputs are the support force and moment, $\mathbf{y}$, while the outputs are the acceleration of the arm joints, $\ddot{\mathbf{q}}_a$. An algebraic input-output relation is determined between the input and output variables (Equation (5.13)) so that a control scheme can be utilized. The controller used in this thesis is the integral

sliding mode control. For integral sliding mode control, a new variable, $\mathbf{z}$ is defined for the input variable.

The input-output relation is considered. New output variables are defined.

$$\ddot{\mathbf{z}} = \mathbf{y}, \quad \dot{\mathbf{z}} = \int_0^t \mathbf{y} dt, \quad \mathbf{z} = \int_0^t \dot{\mathbf{z}} dt. \tag{6.1}$$

Output errors are defined as the difference between the measured and the desired value

$$\tilde{\mathbf{z}} = \mathbf{z} - \mathbf{z}^d, \quad \dot{\tilde{\mathbf{z}}} = \dot{\mathbf{z}} - \dot{\mathbf{z}}^d, \quad \ddot{\tilde{\mathbf{z}}} = \ddot{\mathbf{z}} - \ddot{\mathbf{z}}^d, \tag{6.2}$$

where

$$\ddot{\mathbf{z}}^d = \mathbf{y}^d, \quad \dot{\mathbf{z}}^d = \int_0^t \mathbf{y}^d dt, \quad \mathbf{z}^d = \int_0^t \dot{\mathbf{z}}^d dt. \tag{6.3}$$

The nominal input-output model becomes

$$\ddot{\mathbf{z}} = \mathbf{b}\ddot{\mathbf{q}}_a + \mathbf{f}, \tag{6.4}$$

where $\mathbf{b}$ and $\mathbf{f}$ are defined in Chapter 5, Equation (5.13). A first-order sliding surface is considered below.

$$\begin{aligned} \mathbf{s} &= (\dot{\mathbf{z}} - \dot{\mathbf{z}}^d) + \mathbf{\Lambda}\tilde{\mathbf{z}}, \\ &= \dot{\mathbf{z}} - (\dot{\mathbf{z}}^d - \mathbf{\Lambda}\tilde{\mathbf{z}}), \\ &= \dot{\mathbf{z}} - \mathbf{s}_r, \end{aligned} \tag{6.5}$$

where $\mathbf{\Lambda}$ is 6×6 positive-definite diagonal square matrix. The following stable desired closed-loop system behavior is assumed.

$$\dot{\mathbf{s}} = \ddot{\mathbf{z}} - \dot{\mathbf{s}}_r = -\mathbf{K}\text{sign}(\mathbf{s}), \tag{6.6}$$

where the gain, $\mathbf{K}$, is a diagonal positive definite matrix. The function sign($\mathbf{s}$) returns 1 or -1 for individual elements of $\mathbf{s}$ if the element is greater than zero or less than zero, respectively. This gain will cause $\mathbf{s}$ to vanish, and when $\mathbf{s}$ is zero, Equation (6.5) guarantees that $\tilde{\mathbf{z}}$ and $\dot{\tilde{\mathbf{z}}}$ will tend towards zero. To derive the control law that generates the desired closed-loop system behavior (Equation (6.5) and Equation (6.6)), the nominal input-output model (Equation (Equation 6.4)) is substituted into Equation (Equation 6.6). After solving for the input $\ddot{\mathbf{q}}_a$ it can be shown that

$$\ddot{\mathbf{q}}_a = \mathbf{b}^{-1}(-\mathbf{f} + \dot{\mathbf{s}}_r - \mathbf{K}\text{sign}(\mathbf{s})). \tag{6.7}$$

It must be shown that the control law (Equation (6.7)) can stabilize the actual system when a disturbance exists. It is assumed that the disturbance, $\mathbf{d}$, is a bounded,

unknown force/moment vector acting on the robot's body or limbs. The actual model of the system is

$$\ddot{\mathbf{z}} = \mathbf{b}\ddot{\mathbf{q}}_a + \mathbf{f} + \mathbf{d}. \tag{6.8}$$

One of the goals of the integral sliding mode controller is to ensure that the sliding surface parameters will tend towards zero, despite the existence of disturbances. A Lyapunov function, V, is one that is positive semi-definite, that is

$$V \geq 0. \tag{6.9}$$

Since a first-order stable sliding surface is considered (Equation (6.5)), the Lyapunov function must contain $\mathbf{s}$. A Lyapunov using the norm of $\mathbf{s}$ is used:

$$V = \frac{1}{2}\|\mathbf{s}\|^2 = \frac{1}{2}\mathbf{s}^T\mathbf{s}. \tag{6.10}$$

As long as the time rate of the Lyapunov function is negative at all times, as defined in Equation (6.9), $\mathbf{s}$ will vanish. Here, the condition on controller gain $\mathbf{K}$ is found to guarantee a negative rate for the Lyapunov function. The rate is calculated:

$$\dot{V} = \mathbf{s}^T\dot{\mathbf{s}}. \tag{6.11}$$

$\dot{\mathbf{s}}$ is replaced by Equation (6.5):

$$\dot{V} = \mathbf{s}^T(\ddot{\mathbf{z}} - \dot{\mathbf{s}}_r). \tag{6.12}$$

$\ddot{\mathbf{z}}$ is replaced by Equation (6.8):

$$\dot{V} = \mathbf{s}^T(\mathbf{b}\ddot{\mathbf{q}}_a + \mathbf{f} + \mathbf{d} - \dot{\mathbf{s}}_r). \tag{6.13}$$

$\ddot{\mathbf{q}}_a$ is replaced by Equation Equation 6.7:

$$\dot{V} = \mathbf{s}^T(\mathbf{b}\mathbf{b}^{-1}(-\mathbf{f} + \dot{\mathbf{s}}_r - \mathbf{K}\text{sign}(\mathbf{s})) + \mathbf{d} + \mathbf{f} - \dot{\mathbf{s}}_r). \tag{6.14}$$

After simplification:

$$\begin{aligned} \dot{V} &= \mathbf{s}^T(-\mathbf{K}\text{sign}(\mathbf{s}) + \mathbf{d}) \\ &= -\mathbf{s}^T\mathbf{K}\text{sign}(\mathbf{s}) + \mathbf{s}^T\mathbf{d} \\ &= -\mathbf{K}_v\,|\mathbf{s}| + \mathbf{d}^T\mathbf{s}, \end{aligned} \tag{6.15}$$

where $\mathbf{K}_v$ is a row vector containing the diagonal elements of the diagonal matrix $\mathbf{K}$.

A bound is assumed for the elements of the 6×1 disturbance vector:

$$|d_i| \leq D_i, \quad i = 1, ..., 6. \tag{6.16}$$

Using this, Equation (6.15) becomes

$$\begin{aligned} \dot{V} &\leq -\mathbf{K}_v |\mathbf{s}| + \mathbf{D}^T |\mathbf{s}|, \\ &\leq -(\mathbf{K}_v - \mathbf{D}^T)|\mathbf{s}|. \end{aligned} \tag{6.17}$$

Equation (6.17) implies that if the elements of $\mathbf{K}_v$ are selected such that they are larger than the corresponding elements of $\mathbf{D}^T$, then the rate of the Lyapunov function is negative, and $\mathbf{s}$ vanishes despite the existence of any disturbances that are less than or equal to the disturbance vector. In the form of an equation,

$$\mathbf{K}_v \geq \mathbf{D}^T + \boldsymbol{\eta}^T, \tag{6.18}$$

where $\boldsymbol{\eta}$ is a column vector with positive elements.

6.2 Additional Controller/Switching the Controller

When the controller detects a disturbance, the controller modifies the trajectory of the humanoid's arms to reject the disturbance. This causes the arm trajectory to deviate from the desired trajectory such that the output, the force and moment reactions under the support foot, remains practically equal to the desired output. The disturbance amount can be estimated using the following:

$$\mathbf{y}^d = \mathbf{b}(\mathbf{q}_a^d)\ddot{\mathbf{q}}_a^d + \mathbf{f}(\mathbf{q}_a^d) = \mathbf{b}(\mathbf{q}_a)\ddot{\mathbf{q}}_a + \mathbf{f}(\mathbf{q}_a) + \mathbf{d}. \tag{6.19}$$

Solving for the disturbance gives

$$\mathbf{d} = \mathbf{y}^d - (\mathbf{b}(\mathbf{q}_a)\ddot{\mathbf{q}}_a + \mathbf{f}(\mathbf{q}_a)). \tag{6.20}$$

When the disturbance period is over, this estimation will result in the disturbance $\mathbf{d}$ equalling zero. Using this, an equation similar to that of a mass-spring-damper system can be utilized to make the arm trajectory converge back to the desired arm trajectory:

$$\mathbf{u} = \ddot{\mathbf{q}}_a^d - \mathbf{C}(\dot{\mathbf{q}}_a - \dot{\mathbf{q}}_a^d) - \mathbf{K}_u(\mathbf{q}_a - \mathbf{q}_a^d), \tag{6.21}$$

where $\mathbf{u}$ is the modified arm acceleration $\ddot{\mathbf{q}}_a$, $\mathbf{C}$ is the matrix with damping coefficients on its diagonal, and $\mathbf{K}_u$ is the gain of the switching controller.

With both control schemes defined, the controller can successfully switch between rejecting the disturbance, and returning to the desired trajectory based on the existence of a disturbance. Therefore the total control law is:

$$\mathbf{u} = \begin{cases} \mathbf{b}^{-1}(-\mathbf{f} + \dot{\mathbf{s}}_r - \mathbf{K}\text{sign}(\mathbf{s})) & \text{if} \quad \|d\| \neq 0 \\ \ddot{\mathbf{q}}_a^d - \mathbf{C}(\dot{\mathbf{q}}_a - \dot{\mathbf{q}}_a^d) - \mathbf{K}_u(\mathbf{q}_a - \mathbf{q}_a^d) & \text{if} \quad \|d\| = 0 \end{cases}. \tag{6.22}$$

6.3 Controller Block Diagram

The entire control scheme consists of three subsystems: desired output, disturbance rejection, and the robust joint control. These are shown together in Figure 6.1.

In the subsystem that generates the desired outputs $\mathbf{y}^d$ (the support force and moment components), the nominal trajectories are defined for the joints of the robot's

arms ($\mathbf{q}_a^d(t)$), and the legs and body ($\mathbf{q}_b^d(t)$). These trajectories are designed in such a way that the requirements of a stable walk are met, as described in Chapter 2. To reiterate, these requirements are confining the ZMP within the support polygon during the walking cycle, and keeping the longitudinal and lateral support forces and the support twist moment lower than the maximum static friction between the support foot and the ground. With these requirements met, $\mathbf{y}^d$ will yield a desirable, stable walking gait.

The subsystem that modifies the robot's arm motion ($\mathbf{q}_a$) to maintain the desired output ($\mathbf{y}^d$) contains the disturbance rejection controller. This subsystem receives the desired output and its associated integrals, as well as the measured output, $\mathbf{y}_m$. The measured output is provided by a sensor on the bottom of the robot's foot, similar to that of [30], where force sensors transmit force distribution and moment data. The output of the disturbance rejection control system is the modified arm motion, $\mathbf{q}_a$.

Lastly, the subsystem that controls the motion of the robot's joints is considered. This subsystem receives the desired motion of the body and legs ($\mathbf{q}_b^d(t)$), and the modified arm motion ($\mathbf{q}_a$). The torques of the joints (τ) are calculated from the measured joint positions ($\mathbf{q}_{am}$, $\mathbf{q}_{bm}$) by a robust joint controller, however this particular controller is beyond the focus of this thesis and has no bearing on the outcome of the simulations. This controller must be able to perfectly perform the desired joint motion despite the existence of potential bounded disturbances.

The controller is tested in a similar manner to that demonstrated in [33], however, instead of a two-dimensional 7-DOF robot, a three-dimensional 18-DOF robot is considered.

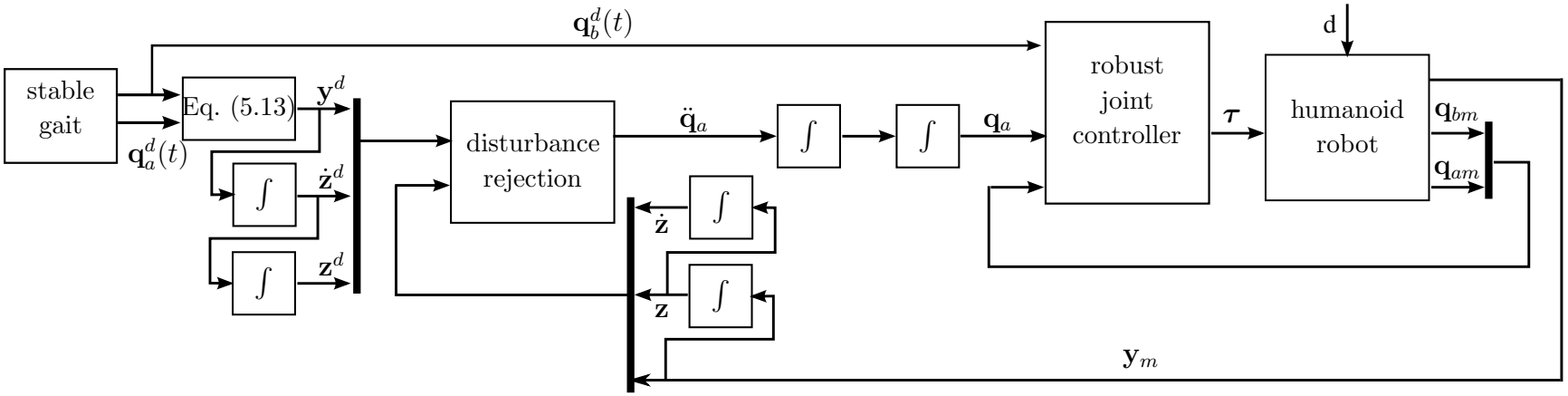

Figure 6.1: Block Diagram

CHAPTER 7

SIMULATIONS

In order to demonstrate the effectiveness of the proposed control method, the 18-DOF robot as described in Chapter 3 is considered. A detailed description of the degrees of freedom is listed below in Table 7.1 and Table 7.2.

The kinematic parameters of each frame, such as the mass, center of mass location, and principal moment of inertia are displayed in Table 7.3 for the legs, and in Table 7.4 for the arms. These values are found from a computer aided design (CAD) rendering of the humanoid using Solid Edge. Approximate uniform densities of each part of the humanoid are obtained by dividing the mass of each part by the respective volume. The mass is found using a digital scale and the volume is calculated by the CAD software. Each frame is assembled separately in the CAD environment, where the total mass, distance to the center of mass (COM), and moment of inertia for each frame are calculated.

As can be seen in Table 7.3 and Table 7.4, the principal moment of inertia values are very small, with the largest being I_1 for q_{b6} at 603.244 $\text{kg} \cdot \text{mm}^2$, equivalent to approximately 6.03×10^{-4} $\text{kg} \cdot \text{m}^2$. As a result, the moment of inertia matrix, $\mathbf{I}_i^B$ defined in Equation (5.12) is assumed to be zero. Additionally, it is assumed that the

Table 7.1: DOF Leg/Body Descriptions

Joint	Joint Description
q_{b1}	Stance Leg Ankle Roll Joint
q_{b2}	Stance Leg Ankle Pitch Joint
q_{b3}	Stance Leg Knee Joint
q_{b4}	Stance Leg Hip Pitch Joint
q_{b5}	Stance Leg Hip Roll Joint
q_{b6}	Stance Leg Hip Yaw Joint
q_{b7}	Swing Leg Hip Yaw Joint
q_{b8}	Swing Leg Hip Roll Joint
q_{b9}	Swing Leg Hip Pitch Joint
q_{b10}	Swing Leg Knee Joint
q_{b11}	Swing Leg Ankle Pitch Joint
q_{b12}	Swing Leg Ankle Roll Joint

Table 7.2: DOF Arm Descriptions

Joint	Joint Description
q_{a1}	Left Arm Shoulder Pitch Joint
q_{a2}	Left Arm Shoulder Roll Joint
q_{a3}	Left Arm Elbow Joint
q_{a4}	Right Arm Shoulder Pitch Joint
q_{a5}	Right Arm Shoulder Roll Joint
q_{a6}	Right Arm Elbow Joint

ZMP location and support forces that correspond to the defined desired trajectory are desirable, and no attempt has been made to minimize the variation of the ZMP position for the defined walking gait obtained from the BIOLOID software.

A disturbance acts upon the robot in a limited period between t_s and t_e in the following form

$$\mathbf{d} = \begin{bmatrix} \mathbf{F}_d(1 - \cos(\frac{2\pi(t-t_s)}{t_e-t_s}))/2 \\ \mathbf{M}_d(1 - \cos(\frac{2\pi(t-t_s)}{t_e-t_s}))/2 \end{bmatrix}, \quad t_s \leq t \leq t_e, \tag{7.1}$$

Table 7.3: Leg/Body Frame Parameters

Frame	Mass (kg)	Distance to CoM (mm)			Moment of Inertia ($\mathrm{kg \cdot mm^2}$)		
		x	y	z	I_1	I_2	I_3
1	0.125	12.713	0.359	-16.072	69.178	58.741	33.507
2	0.076	65.007	-11.357	0.590	41.100	40.801	23.853
3	0.022	33.232	-7.186	0.000	18.724	12.332	10.158
4	0.125	-12.712	16.072	0.360	69.179	58.741	33.507
5	0.011	-0.002	18.936	-16.483	10.726	10.256	2.151
6	0.321	39.355	-11.382	84.731	603.244	375.464	304.179
7	0.011	0.002	-16.483	18.936	10.726	10.256	2.151
8	0.125	-0.359	-16.071	-12.713	69.162	58.740	33.507
9	0.022	43.157	7.263	0.000	18.724	12.332	10.158
10	0.076	11.382	11.281	-0.590	41.054	40.756	23.852
11	0.125	12.712	16.072	-0.359	69.179	58.741	33.507
12	0.032	-25.804	4.754	-0.001	37.324	31.291	10.328

Table 7.4: Arm Frame Parameters

Frame	Mass (kg)	Distance to CoM (mm)			Moment of Inertia ($\mathrm{kg \cdot mm^2}$)		
		x	y	z	I_1	I_2	I_3
1L	0.009	3.781	0.000	-12.232	4.191	3.515	1.607
2L	0.069	18.536	-0.001	0.664	33.057	27.783	13.039
3L	0.074	22.432	0.840	0.620	48.150	44.834	12.026
1R	0.009	3.781	0.000	-12.232	4.191	3.515	1.607
2R	0.069	18.536	0.001	0.664	33.057	27.783	13.039
3R	0.074	22.432	-0.840	0.618	48.450	44.835	12.025

where $\mathbf{F}_d$ is a 3×1 disturbance force vector describing a disturbance force acting in the x, y, and z directions with respect to the base frame. Similarly, $\mathbf{M}_d$ is a 3×1 disturbance moment vector describing the disturbance moment acting about the x, y, and z axes with respect to the base frame. t_s and t_e are the start and end times of the disturbance, respectively. In this example, a smooth varying force of 1.349 N (10% of the robot's total weight) is applied on the robot's body at a height of 0.274 m

(75% of the robot's total height). The disturbance acts on the robot at $t_s = 0.00$ s until $t_e = 0.02$ s.

To get a better sense of this disturbance, the force can be equated to the completely elastic collision of a ball of mass 0.01 kg moving at a particular velocity. This collision occurs at the same point on the robot's body as the original disturbance force. The collision can be approximated by taking the integral of the force versus time, as shown below:

$$L = \int_{t_s}^{t_e} F_d(1 - \cos(\frac{2\pi(t - t_s)}{t_e - t_s}))/2 \quad dt. \tag{7.2}$$

Evaluating the integral gives,

$$L = \frac{F_d}{2}(t_e - t_s) = \frac{F_d}{2}\Delta t. \tag{7.3}$$

This is equated to the change in momentum of a ball,

$$L = m_{ball}(v_2 - v_1), \tag{7.4}$$

where v_1 is the initial impact velocity and v_2 is the bounce back velocity after the impact. Assuming a completely elastic collision, the velocity before and after the impact are equal with opposite directions, that is $v_1 = -v_2$. This velocity is renamed v for simplicity. Simplifying Equation (7.4) gives

$$L = 2m_{ball}v. \tag{7.5}$$

Substituting Equation (7.3) into Equation (7.5) gives the following:

$$\frac{F_d}{2}\Delta t = 2mv. \tag{7.6}$$

By solving Equation (7.6) for the ball's velocity, the equivalent velocity of a ball impacting the robot is

$$v = \frac{F_d \Delta t}{4m}. \tag{7.7}$$

Using the values of the simulation, the disturbance force can be equated to a ball of mass 0.01 kg impacting the robot with a velocity of approximately 0.675 $\frac{\text{m}}{\text{s}}$ at the same point of impact as the disturbance force.

This disturbance can easily cause an unstable walk when a disturbance rejection controller is not used. A comparison of the effect of this disturbance in both controlled and uncontrolled cases is shown in Figure 7.1 and Figure 7.2 for the first 0.1 second of the simulation. By implementing the controller described in Chapter 6, the disturbance is successfully rejected. Figure 7.3 and Figure 7.4 show the controller output for the full duration of the simulation.

The disturbance rejection controller modifies the original trajectories of the arms in order to compensate for the disturbance. In Figure 7.5 and Figure 7.6, the controller uses a slight motion of the arms to compensate for the disturbance force described above.

The robot walks in three dimensions and therefore the ZMP moves in the two-dimensional plane of the foot, in the case of robot discussed in this thesis, the y

and z directions. The ZMP in both directions is determined by Equation (2.1) and Equation (2.2). The trajectory of the ZMP for both controlled and uncontrolled cases, compared to the desired trajectory is shown in Figure 7.7 for the y-direction and for the z-direction. The shift in the ZMP in both cases is determined by taking the difference of the uncontrolled and controlled disturbed cases, with the undisturbed case. This is shown in Figure 7.8 for the y and z directions. By examining the figures, it can be seen that when the controller is not used, the ZMP shifts a maximum of 0.000 mm along the y-axis, and 27.9 mm along the z-axis when a disturbance occurs in the uncontrolled case. This shift is significant enough to cause the humanoid's walking gait to become unstable, potentially causing the robot to tip and fall. The inclusion of the disturbance rejection controller allows the robot to recover from the disturbance force and maintain a stable walking gait. As a result, the maximum ZMP shift along the y-axis is 2.104 mm and 5.866 mm along the z-axis. The increase in the shift along the y-axis is due to the controller compensating for the disturbance and converging back to the desired trajectory. The disturbance is small and does not cause any significant harm to the stability of the robot's walk.

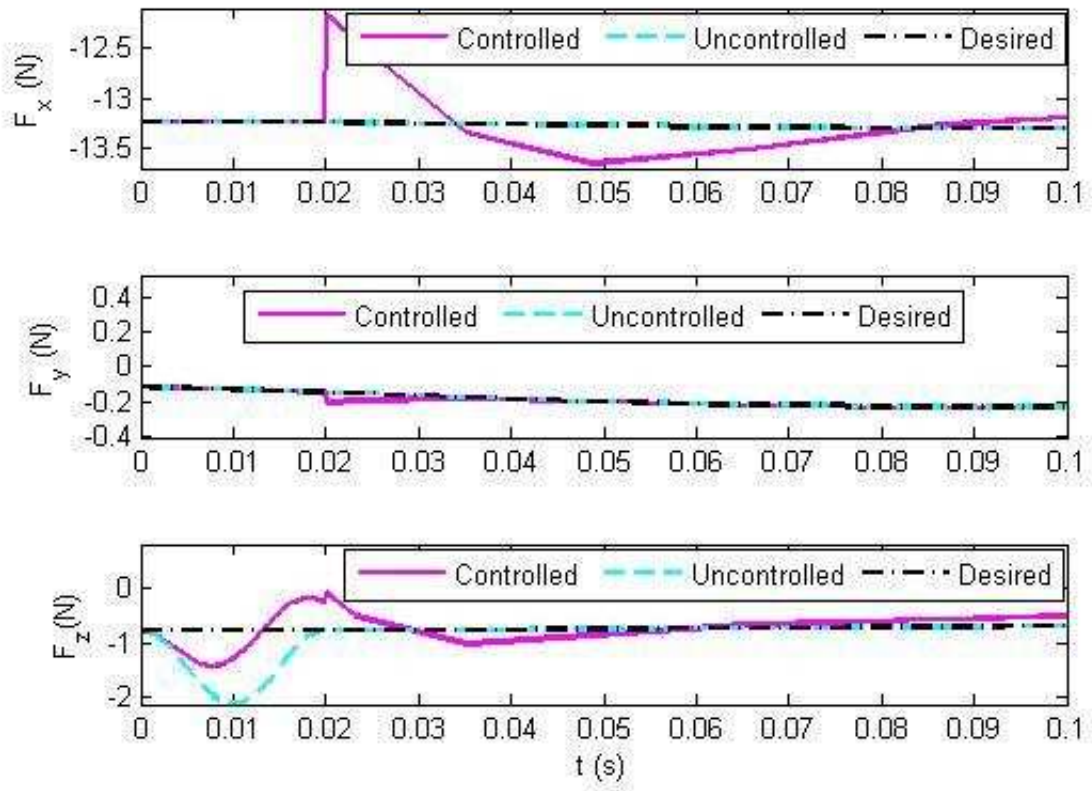

Figure 7.1: Effect of the disturbance on the support force for controlled and uncontrolled cases. y_1 is the vertical support force F_x, y_2 is the lateral support force F_y, y_3 is the longitudinal support force F_z. Shown from $0 \leq t \leq 0.1$.

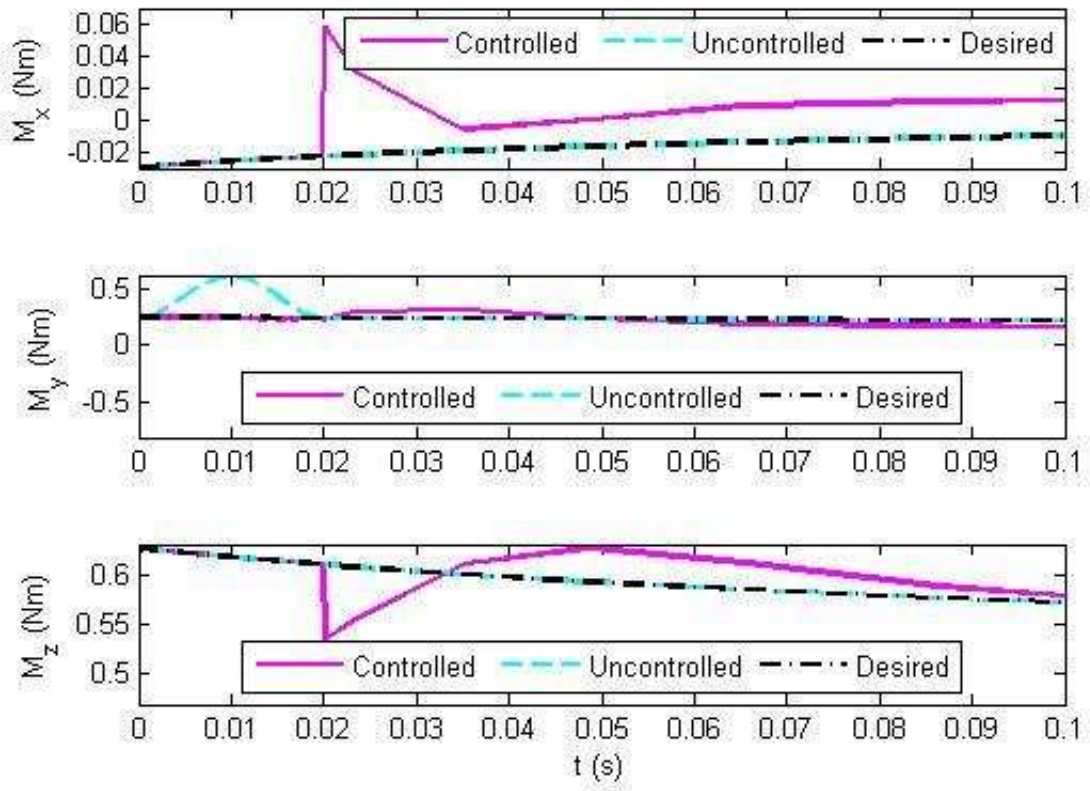

Figure 7.2: Effect of the disturbance on the support moment for controlled and uncontrolled cases. y_4 is the vertical twist moment M_x, y_5 is the moment about the longitudinal axis M_y, y_6 is the moment about the lateral direction M_z. Shown from $0 \leq t \leq 0.1$.

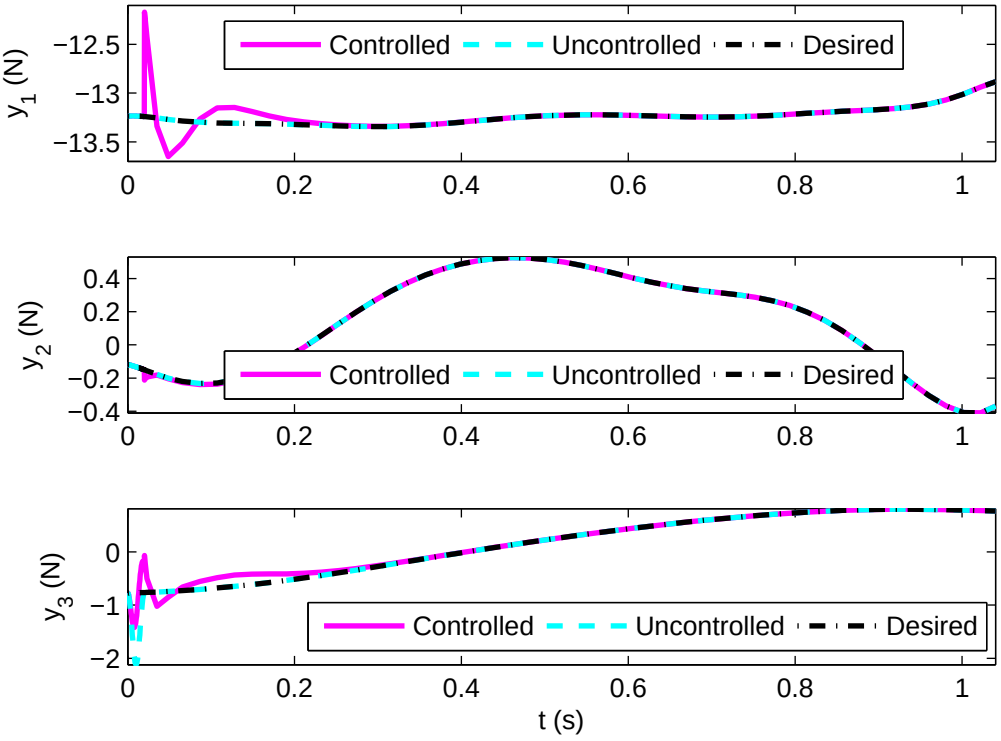

Figure 7.3: Effect of the disturbance on the support force for controlled and uncontrolled cases. y_1 is the vertical support force F_x, y_2 is the lateral support force F_y, y_3 is the longitudinal support force F_z.

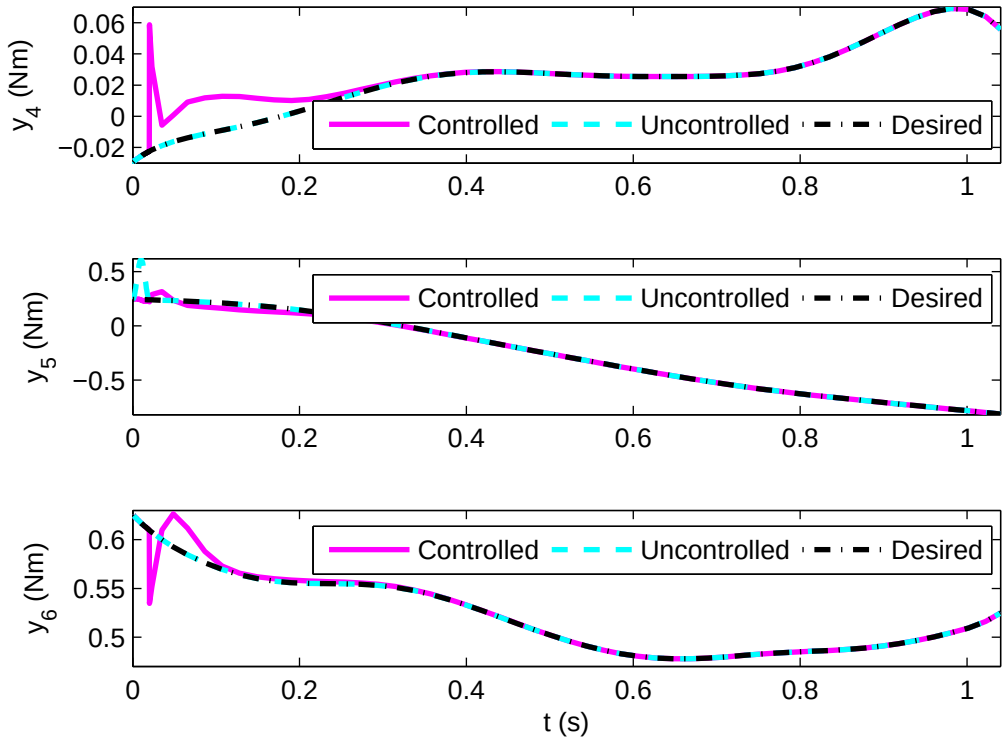

Figure 7.4: Effect of the disturbance on the support moment for controlled and uncontrolled cases. y_4 is the vertical twist moment M_x, y_5 is the moment about the longitudinal axis M_y, y_6 is the moment about the lateral direction M_z.

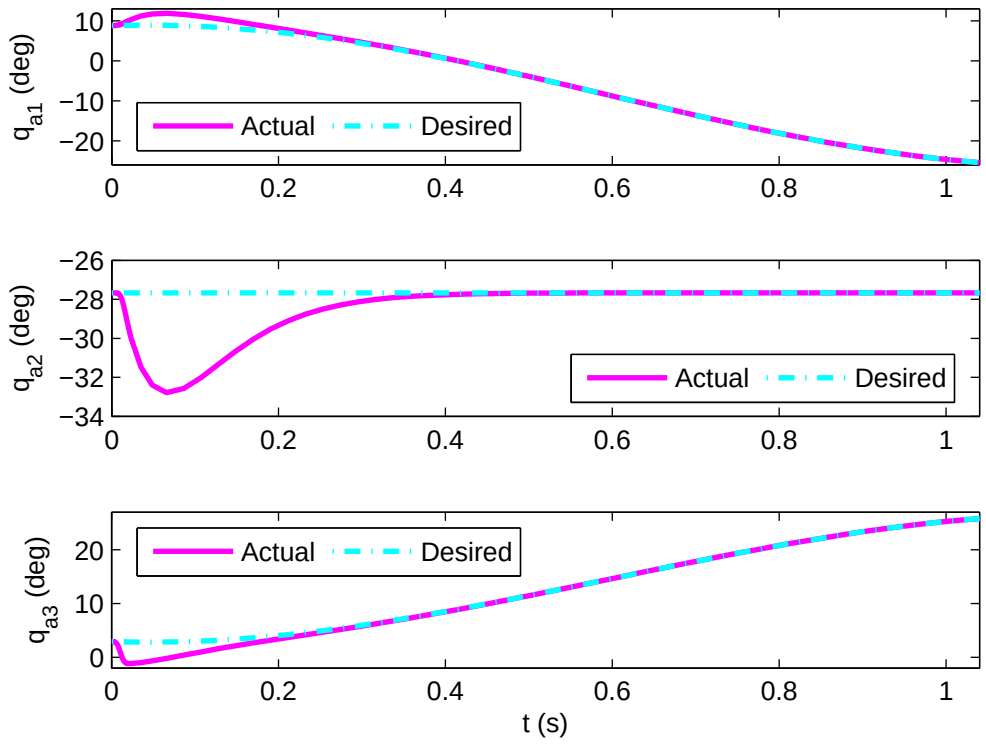

Figure 7.5: Modified trajectory of the left arm joint vs their desired trajectory.

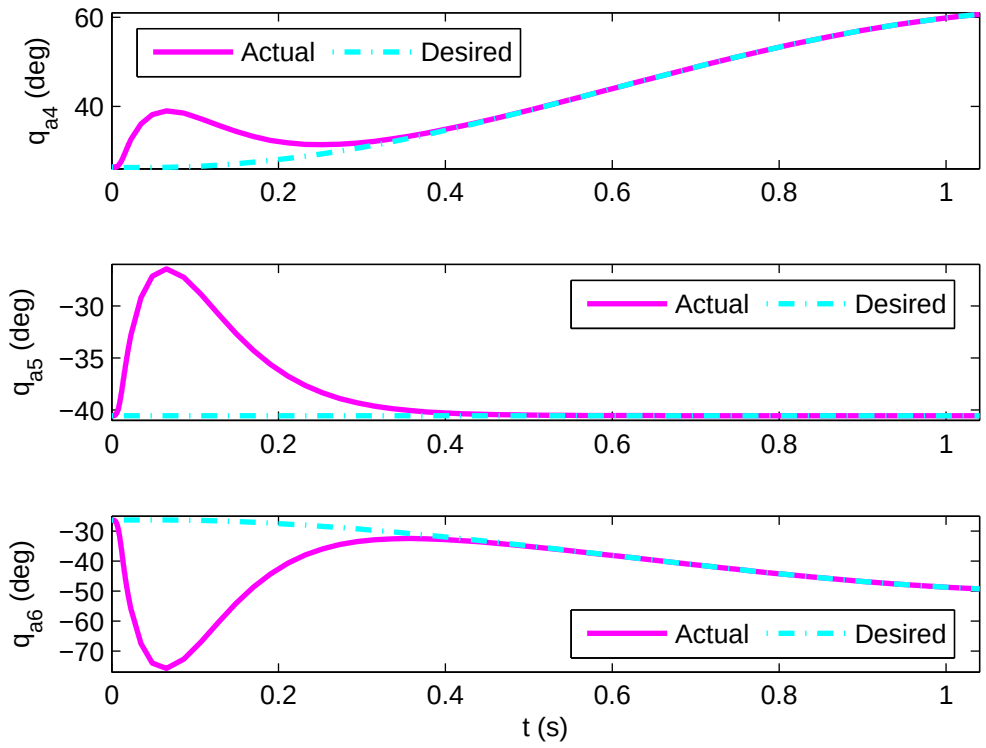

Figure 7.6: Modified trajectory of the right arm joints vs their desired trajectory.

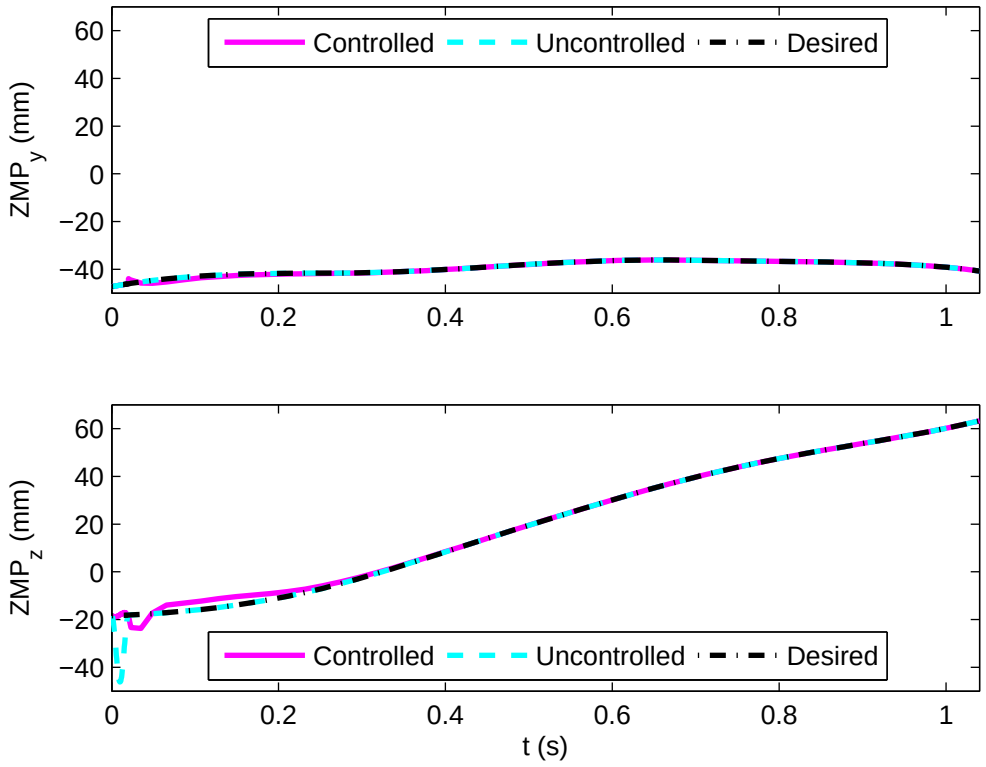

Figure 7.7: Effect of the disturbance on the ZMP for controlled and uncontrolled cases.

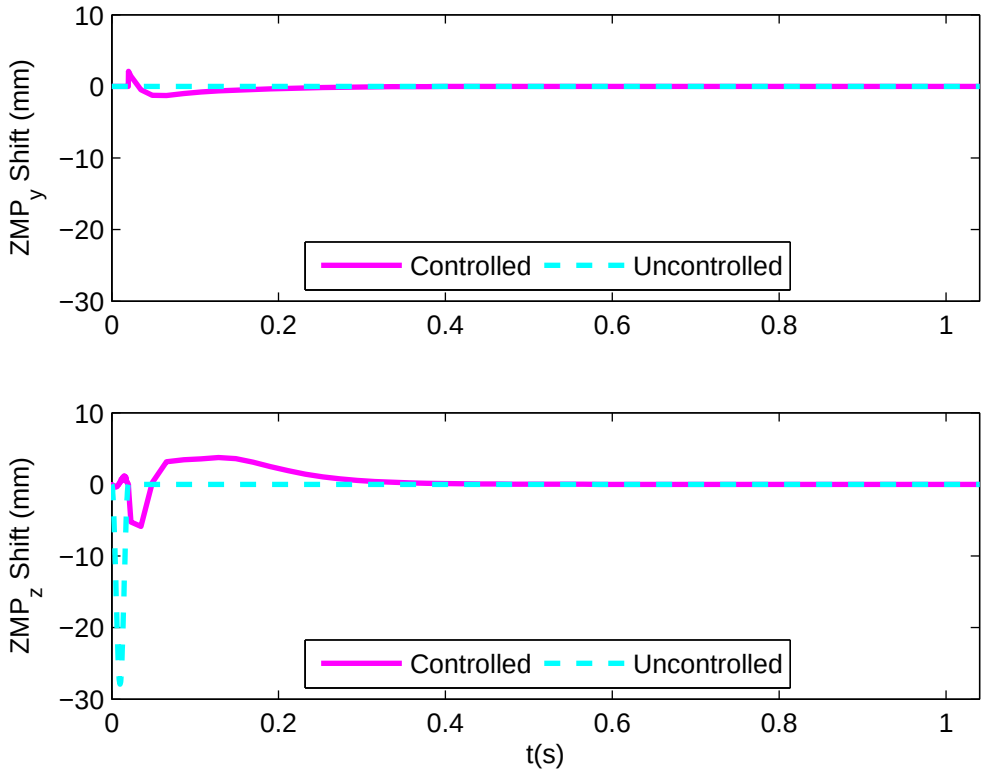

Figure 7.8: Effect of the disturbance on the shift in the ZMP.

CHAPTER 8

CONCLUSION

A disturbance rejection controller is proposed in general form based on three dimensional kinematics for biped robots, and applied to an 18-DOF biped humanoid robot with 12-DOF for the legs and body, and 6-DOF for the arms. The swing phase of the robot's walking gate is considered. A sliding mode architecture is chosen for the disturbance rejection, where the support forces and moments of the support foot are chosen as the outputs, with the acceleration of the arm joints is chosen for the inputs. It is assumed that the support forces and moments are gathered from force sensors mounted on a "shoe" on the bottom of the robot's feet. The position, velocity, and acceleration of the joints are gathered from the servo motors in the robot. As can be seen from the simulations in Chapter Chapter 7, the controller successfully mitigates bounded disturbances to maintain the desired support force and moments. However, reducing the shift in the ZMP along the y and z axes is given priority versus fast convergence to the desired values. By keeping the shift in ZMP low, the robot maintains a more stable walking gait. If, instead, fast convergence is chosen, the shift in ZMP increases, thereby increasing the possibility of an unstable situation during the robot's gait.

During the disturbance rejection, only the arms joints deviate from their desired trajectory, while the leg and body joints remain at their desired trajectory. This has important implications during tasks where foot placement or specific leg/body positions are critical, i.e. the stepping stone problem. Since the leg and body joint trajectories are unaffected, the robot will still be able to complete the task, even when bounded disturbances are experienced.

The controller utilizes the full kinematic model of the BIOLOID robot. This provides an accurate representation of the robot's gait and its reactions to forces. Unfortunately, modeling the full model of the robot is computationally intensive, and calculations become slow. This makes the likelihood of real-time implementation a smaller possibility without streamlining the calculations. Unless the model is simplified, or computational speed increases significantly, the current model may only be restricted to off-line calculation. Additionally, because the method of disturbance rejection involves deviating the arms from their desired trajectory, tasks where arm trajectory is paramount, such as when the robot is carrying an object in its arms, this method of disturbance rejection may not be the best choice.

This thesis encompasses only the simulations of the robot. Future work will include testing the controller on the BIOLOID hardware. Additionally, the "shoe" with the necessary force sensors will be created and attached to the robot. To address the intensive computations, the model may be simplified so that real-time implementation becomes possible.

Overall, this thesis shows that using a sliding mode architecture to reject bounded disturbances by only modifying the accelerations of the arm joints is a successful approach to biped humanoid walking.

APPENDIX

SUPPORTING ASME PUBLICATION

Proceedings of the ASME 2011 International Mechanical Engineering Congress & Exposition
IMECE2011
November 11-17, 2011, Denver, Colorado, USA

IMECE2011-62270

ACTIVE DISTURBANCE REJECTION FOR BIPEDAL WALK OF A HUMANOID ROBOT USING THE MOTIONS OF THE ARMS

Joshua Hill and Farbod Fahimi
Department of Mechanical and Aerospace Engineering
UAHuntsville
Huntsville, Alabama 35899
Email: fahimi@eng.uah.edu

ABSTRACT

A control system for the walking of a redundant biped robot in the swing phase is considered. The biped is a humanoid with 6DOF per leg and 3DOF per arm. The controller will be based on a full kinematic model of the robot to depict a more accurate behavior of the robot. The arms of the robot are used to compensate for disturbances the robot may experience during walking. Instead of controlling the robots ZMP, keeping it within the support polygon, all six foot support reaction components are controlled. First, a "shoe" with force sensors detect the forces and moments on the foot for feedback. The feedback from the joint servos provide position and velocity information. The support reaction and the joint position/velocities are fedback to a sliding mode controller, which makes adjustments to the arm links' acceleration to compensate the shift in the reaction components. Simulations show the comparison of the ZMP shift when disturbances are applied with and without controlling the reaction forces to prove the effectiveness of the approach.

NOMENCLATURE

d Unknown actual disturbance vector
D Upper bound of actual disturbance vector
$\mathbf{F}_R$ Actual force vector exerted by robot to ground
$\mathbf{F}_R^d(t)$ Desired force vector exerted by robot to ground
$\mathbf{F}_s$ Actual force vector exerted by ground to robot
F_x Longitudinal support force
F_y Lateral support force
F_z Vertical support force
g Gravitational acceleration vector
$\mathbf{G}_{ai}$ Jacobian matrix for arm joint angular velocities
$\mathbf{G}_{bi}$ Jacobian matrix for body/legs joint angular velocities
$\mathbf{I}_i^B$ Link *i* moment of inertia matrix expressed in local frame
$\mathbf{J}_{ai}$ Jacobian matrix for arm joint linear velocities
$\mathbf{J}_{bi}$ Jacobian matrix for body/legs joint linear velocities
K Diagonal positive definite gain matrix
$\mathbf{K}_v$ Row vector containing the diagonal elements of **K**
m_i Mass of link *i*
$\mathbf{M}_R$ Actual moment vector exerted by robot to ground
$\mathbf{M}_R^d(t)$ Desired moment vector exerted by robot to ground
$\mathbf{M}_s$ Actual moment vector exerted by ground to robot
M_x Support moment about the longitudinal axis
M_y Support moment about the lateral axis
M_z Support moment about the vertical axis
q Joint variables of the robot's limbs
$\mathbf{q}_a$ Vector containing arm joint positions
$\mathbf{q}_b$ Vector containing body/legs joint positions
$\mathbf{q}^d(t)$ Desired joint variables of the robot's limbs
$\mathbf{R}_{0i}$ Transformation from local frame of link *i* to inertial frame
$\mathbf{r}_i$ Position vector of the center of gravity of link *i*
s Parameter defining the surface for sliding mode control
u Control input - vector containing arm joint accelerations
y Actual control output
$\mathbf{y}^d$ Desired control output
z Double time integral of control output
ω_i Link *i* angular velocity vector expressed in global frame
ω_i^B Link *i* angular velocity vector expressed in local frame

Introduction

For stable dynamic locomotion, the necessary and sufficient condition is to have the ZMP (Zero Moment Point) within the area on the ground covered by the feet during locomotion (support polygon) [1].

The first ZMP-based approach for biped walking control involves defining the desired trajectory of the biped joints such that the ZMP remains in the support polygon at all times. This approach has been used for Manus-I [2] and the Honda Asimo Robot [3]. In this approach, there is no closed-loop control ensuring that the ZMP remains in the support polygon when an external disturbance is present, which may lead to instability in presence of a disturbance.

The second approach is the ZMP compensation via feedback, in which the *joint torques* or *joint trajectories* are modified in real-time according to disturbances to keep the ZMP within the support polygon.

As an example of the use of *joint torques*, injecting compensating torque into the ankle-joint of the foot of a robot for ZMP control is demonstrated in [4].

Several methods have been proposed for modification of *joint trajectories* for ZMP control. In most works, the *position* of joints are modified. Altering the speed of walk, which affects timing of joint trajectories has been proposed [5]. Modification of the motion of the robot's trunk and waist [6–8], or the robot's base link of the stance leg [9] have been introduced. Normally, simplified models of the robot are used for calculation of the robot's trunk and waist modified motions. It is common to model the whole multi-DOF (Degree-Of-Freedom) robot as an inverted pendulum (e.g. [10]). Recently, methods have been proposed that modify the *acceleration* of joints. Acceleration of the robot's torso [11] and upper-limbs via feedback linearization [12] have been used for ZMP control.

It can be seen that most of the research in dynamic stabilization of humanoid robots have focused on using only the ZMP as an indication of dynamic stability. However, the ZMP position only represents three support reaction components, namely one vertical force and two lateral and longitudinal moment components. When a disturbance exists or when the motion of a limb is modified to compensate for an existing disturbance, the lateral and longitudinal support force and the vertical support moment are also affected. These support reaction components are normally provided by friction, which is limited. Excessive lateral and longitudinal support force and the vertical support moment lead to foot sliding, which can cause a fall. So, in some cases, controlling only the ZMP position is not sufficient to maintain dynamic stability.

In this paper, instead of controlling only the position of the ZMP, all the force and moment components of the support foot reaction are controlled. This way, not only the tipping of the robot is addressed, but also *the sliding of the support foot* is prevented under bounded disturbances. Since a total of 6 components of the support reaction are controlled, 6 DOFs of the arms of the robot must be used for control. Here, the acceleration of joints are used as control inputs, unlike more common approaches in which position of joints are used.

Approach

A humanoid robot is considered. The joint variables of the robot's limbs are denoted by $\mathbf{q}$. The gait of the robot during one swing phase is considered. The desired joint trajectories $\mathbf{q}^d(t)$ for the swing phase are defined such that they constitute a stable walk. To constitute a stable walk, the desired joint trajectories must meet two conditions: *a*) The position of ZMP must always be within the support polygon; *b*) The longitudinal and lateral support force (F_x, F_y) and the vertical twist moment (M_z) of the support foot must meet the limitation of the static friction between the foot and the ground. Note that the ZMP position is a function of the vertical force on the foot (F_z) and the lateral and longitudinal moments (M_x, M_y). So, meeting the two requirements *a* and *b* is equivalent to maintaining a desired support force vector ($\mathbf{F}_R^d(t)$) and moment vector ($\mathbf{M}_R^d(t)$) during the walk, where

$$\mathbf{F}_R = [F_x, F_y, F_z]^T, \quad \mathbf{M}_R = [M_x, M_y, M_z]^T. \tag{1}$$

The desired support force and moment vectors are the ones that exist when the robot is walking on a perfectly level ground with no disturbance. They are calculated based on the joint trajectories of a stable walk.

It is assumed that during the walk, bounded disturbances exist. Examples of disturbances are external forces/moment acting on the robot's body, or slight unevenness of the ground. The disturbances affect the support force and moment vectors.

It is proposed to design a feedback controller to control the support force and moment vectors in real-time to keep them at their desired values despite the existence of disturbances. So, the control output is defines as

$$\mathbf{y} = \begin{bmatrix} \mathbf{F}_R \\ \mathbf{M}_R \end{bmatrix}, \tag{2}$$

with the desired value

$$\mathbf{y}^d(t) = \begin{bmatrix} \mathbf{F}_R^d(t) \\ \mathbf{M}_R^d(t) \end{bmatrix}. \tag{3}$$

It is desirable to correct the motion of the robot's arm joints around their desired trajectory to compensate for bounded external disturbances applied over a small time period. The arms of

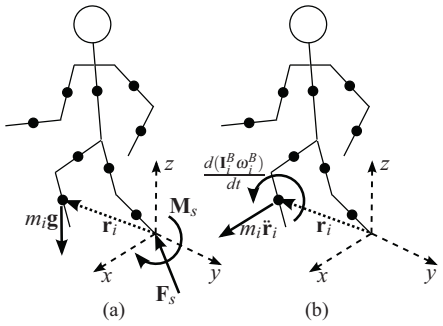

FIGURE 1. a) FREE BODY DIAGRAM, b) KINETIC DIAGRAM

the robot have a total of 6 DOFs, three DOFs per arm. The acceleration of the arm joints ($\ddot{\mathbf{q}}_a$, which is a 6×1 vector) affects the support force and moment vector. So, this acceleration vector is considered the control input ($\mathbf{u}=\ddot{\mathbf{q}}_a$).

This control input is integrated in real-time to generate alternative desired trajectories for the arms, while the desired trajectories of the robot's body and leg joints remain unchanged. Then, an independent control layer controls the joints of the arms, legs, and body of the robot to follow their desired trajectory.

For the control design, an input-output relation is necessary. First, this relation is derived. Then, a sliding mode controller is designed based on the input-output model and tested by simulation.

Input-Output Model

The external forces and moments that act on the robot as a system of rigid bodies at time t are shown in Fig. 1a. The resultant inertia forces and moments at time t are shown in Fig. 1b. The robot is in a state of dynamic balance at time t. So, one can write:

$$\mathbf{F}_s+\sum m_i\mathbf{g}=\sum m_i\ddot{\mathbf{r}}_i, \tag{4}$$

$$\mathbf{M}_s+\sum \mathbf{r}_i\times m_i\mathbf{g}=\sum(\mathbf{R}_{0i}\tfrac{d}{dt}(\mathbf{I}_i^B\omega_i^B)+\mathbf{r}_i\times m_i\ddot{\mathbf{r}}_i), \tag{5}$$

where $\mathbf{F}_s$ and $\mathbf{M}_s$ are the support force and moment from the ground to the robot's foot, respectively. m_i and $\mathbf{I}_i^B$ are the mass and centroid moment of inertia matrix defined in local frame B for link i of the robot, respectively. ω_i^B is the angular velocity of link i in its local frame. $\mathbf{r}_i$ is the global position vector of the centroid of link i. And $\mathbf{R}_{0i}$ converts the local frame of link i to the inertial frame 0.

Noting that the force and moment that the robot foot exerts on the ground ($\mathbf{F}_R$ and $\mathbf{M}_R$) are equal and opposite to those exerted from the ground to the robot's foot ($\mathbf{F}_s$ and $\mathbf{M}_s$), one can write the following relations.

$$\mathbf{F}_R=\sum(m_i\mathbf{g}-m_i\ddot{\mathbf{r}}_i), \tag{6}$$

$$\mathbf{M}_R=\sum(\mathbf{r}_i\times m_i\mathbf{g}-\mathbf{R}_{0i}(\mathbf{I}_i^B\dot{\omega}_i^B+\omega_i^B\times\mathbf{I}_i^B\omega_i^B)-\mathbf{r}_i\times m_i\ddot{\mathbf{r}}_i). \tag{7}$$

The linear velocity of the center of mass of link i expressed in the inertial frame ($\dot{\mathbf{r}}_i$) is derived in terms of the joint rate vector using Jacobian matrices.

$$\dot{\mathbf{r}}_i=\begin{bmatrix}\mathbf{J}_{ai}\ \mathbf{J}_{bi}\end{bmatrix}\begin{bmatrix}\dot{\mathbf{q}}_a\\ \dot{\mathbf{q}}_b\end{bmatrix}\quad i=1,\ldots,n \tag{8}$$

In Eq. (8), $\dot{\mathbf{q}}_a$ (6×1) and $\dot{\mathbf{q}}_b$ (12×1) are the joint rates for the robot's 6 arm joints and 12 legs/body joints, respectively. $\mathbf{J}_{ai}$ (3×6) and $\mathbf{J}_{bi}$ (3×12) are Jacobian matrices. A similar relation is written for the angular velocity vector of robot's links expressed in the inertial frame (ω_i).

$$\omega_i=\begin{bmatrix}\mathbf{G}_{ai}\ \mathbf{G}_{bi}\end{bmatrix}\begin{bmatrix}\dot{\mathbf{q}}_a\\ \dot{\mathbf{q}}_b\end{bmatrix}\quad i=1,\ldots,n \tag{9}$$

$\mathbf{G}_{ai}$ (3×6) and $\mathbf{G}_{bi}$ (3×12) are Jacobian matrices. The linear and angular accelerations are found by taking derivatives of Eqs. (8) and (9), respectively.

$$\begin{aligned}\ddot{\mathbf{r}}_i&=\mathbf{J}_{ai}\ddot{\mathbf{q}}_a+(\dot{\mathbf{J}}_{ai}\dot{\mathbf{q}}_a+\mathbf{J}_{bi}\ddot{\mathbf{q}}_b+\dot{\mathbf{J}}_{bi}\dot{\mathbf{q}}_b)\\&=\mathbf{J}_{ai}\ddot{\mathbf{q}}_a+\mathbf{f}_{ti}\end{aligned} \tag{10}$$

$$\begin{aligned}\dot{\omega}_i&=\mathbf{G}_{ai}\ddot{\mathbf{q}}_a+(\dot{\mathbf{G}}_{ai}\dot{\mathbf{q}}_a+\mathbf{G}_{bi}\ddot{\mathbf{q}}_b+\dot{\mathbf{G}}_{bi}\dot{\mathbf{q}}_b)\\&=\mathbf{G}_{ai}\ddot{\mathbf{q}}_a+\mathbf{f}_{ri}\end{aligned} \tag{11}$$

Equations (10) and (11) are substituted in Eqs. (6) and (7), respectively, and the results are rearranged to yield

$$\begin{aligned}\mathbf{F}_R&=(-\sum m_i\mathbf{J}_{ai})\ddot{\mathbf{q}}_a+(\sum m_i(\mathbf{g}-\mathbf{f}_{ti}))\\&=\mathbf{b}_f\ddot{\mathbf{q}}_a+\mathbf{f}_f\end{aligned} \tag{12}$$

$$\begin{aligned}\mathbf{M}_R&=[-\sum(\mathbf{R}_{0i}\mathbf{I}_i^B\mathbf{G}_{ai}+m_i\mathbf{r}_i\times\mathbf{J}_{ai})]\ddot{\mathbf{q}}_a\\&\quad+[\sum(m_i\mathbf{r}_i\times\mathbf{g}-\mathbf{R}_{0i}(\omega_i^B\times\mathbf{I}_i^B\omega_i^B+\mathbf{I}_i^B\mathbf{f}_{ri})-m_i\mathbf{r}_i\times\mathbf{f}_{ti}]\\&=\mathbf{b}_m\ddot{\mathbf{q}}_a+\mathbf{f}_m\end{aligned} \tag{13}$$

Finally, Eqs. (12) and (13) are integrated to form the complete input-output equation.

$$\begin{bmatrix}\mathbf{F}_R\\ \mathbf{M}_R\end{bmatrix} = \begin{bmatrix}\mathbf{b}_f\\ \mathbf{b}_m\end{bmatrix}\ddot{\mathbf{q}}_a + \begin{bmatrix}\mathbf{f}_f\\ \mathbf{f}_m\end{bmatrix}$$
$$\mathbf{y} = \mathbf{b}\ddot{\mathbf{q}}_a + \mathbf{f} \tag{14}$$

Note that $\mathbf{b}_f$, $\mathbf{f}_f$, $\mathbf{b}_m$, and $\mathbf{f}_m$ are functions of $\mathbf{q}_a$, $\mathbf{q}_b$, $\dot{\mathbf{q}}_a$, $\dot{\mathbf{q}}_b$, and $\ddot{\mathbf{q}}_b$, which are available for feedback via processing data from the joint position encoders.

It is assumed that independent robust joint controllers drive the joints on their desired trajectory. So, the 12 joints of the body/legs follow their desired trajectory by use of independent robust controllers (i.e., $\mathbf{q}_b = \mathbf{q}_b^d(t)$). Now, a modified $\ddot{\mathbf{q}}_a$ (desired arm joints' acceleration) must be calculated by a "disturbance rejection" control law based on the input-output model (14) to control the support force and moment vectors ($\mathbf{y}$) at their desired values that warrant a stable walk. The modified desired trajectory of the 6 arm joints are derived by integration of $\ddot{\mathbf{q}}_a$, and are realized by an independent robust joint controller.

Disturbance Rejection Control Law

The input-output relation (14) is considered. A new variable is defined.

$$\ddot{\mathbf{z}} = \mathbf{y}, \quad \dot{\mathbf{z}} = \int_0^t \mathbf{y}dt, \quad \mathbf{z} = \int_0^t \dot{\mathbf{z}}dt. \tag{15}$$

Output errors are defined

$$\tilde{\mathbf{z}} = \mathbf{z} - \mathbf{z}^d, \quad \dot{\tilde{\mathbf{z}}} = \dot{\mathbf{z}} - \dot{\mathbf{z}}^d, \quad \ddot{\tilde{\mathbf{z}}} = \ddot{\mathbf{z}} - \ddot{\mathbf{z}}^d, \tag{16}$$

where

$$\ddot{\mathbf{z}}^d = \mathbf{y}^d, \quad \dot{\mathbf{z}}^d = \int_0^t \mathbf{y}^d dt, \quad \mathbf{z}^d = \int_0^t \dot{\mathbf{z}}^d dt. \tag{17}$$

The nominal input-output model becomes

$$\ddot{\mathbf{z}} = \mathbf{b}\ddot{\mathbf{q}}_a + \mathbf{f} \tag{18}$$

A first-order stable sliding surface is considered

$$\begin{aligned}\mathbf{s} &= (\dot{\mathbf{z}} - \dot{\mathbf{z}}^d) + \Lambda^T\tilde{\mathbf{z}},\\ &= \dot{\mathbf{z}} - (\dot{\mathbf{z}}^d - \Lambda^T\tilde{\mathbf{z}}),\\ &= \dot{\mathbf{z}} - \mathbf{s}_r\end{aligned} \tag{19}$$

where Λ is a column vector with all positive elements. The following stable desired closed-loop system behavior is assumed.

$$\dot{\mathbf{s}} = \ddot{\mathbf{z}} - \dot{\mathbf{s}}_r = -\mathbf{K}\text{sign}(\mathbf{s}), \tag{20}$$

in which $\mathbf{K}$ is a diagonal positive definite matrix. The gain $\mathbf{K}$ causes $\mathbf{s}$ to vanish. When $\mathbf{s}$ is zero, Eq. (19) guarantees that $\tilde{\mathbf{z}}$ and $\dot{\tilde{\mathbf{z}}}$ tend to zero.

The control law that generates the desired closed-loop system behavior (20) is derived by substituting the nominal input-output model (18) in (20) and solving for the input.

$$\ddot{\mathbf{q}}_a = \mathbf{b}^{-1}(-\mathbf{f} + \dot{\mathbf{s}}_r - \mathbf{K}\text{sign}(\mathbf{s})) \tag{21}$$

It must be shown that the control law (21) can stabilize the actual system when disturbance exists. A bounded unknown force/moment disturbance vector ($\mathbf{d}$) acting on the robot's body or limbs is assumed. The actual model of the system is

$$\ddot{\mathbf{z}} = \mathbf{b}\ddot{\mathbf{q}}_a + \mathbf{f} + \mathbf{d}. \tag{22}$$

A Lyapunov function is defined.

$$V = \frac{1}{2}\mathbf{s}^T\mathbf{s} \tag{23}$$

For $\mathbf{s}$ to vanish despite disturbances, the time rate of the Lyapunov function must be negative at all times. Here, condition on $\mathbf{K}$ is found to guarantee a negative rate for Lyapunov function. The rate is calculated.

$$\begin{aligned}\dot{V} &= \mathbf{s}^T\dot{\mathbf{s}}\\ &= \mathbf{s}^T(\ddot{\mathbf{z}} - \dot{\mathbf{s}}_r)\\ &= \mathbf{s}^T(\mathbf{b}\ddot{\mathbf{q}}_a + \mathbf{f} + \mathbf{d} - \dot{\mathbf{s}}_r)\\ &= \mathbf{s}^T(\mathbf{b}\mathbf{b}^{-1}(-\mathbf{f} + \dot{\mathbf{s}}_r - \mathbf{K}\text{sign}(\mathbf{s})) + \mathbf{d} + \mathbf{f} - \dot{\mathbf{s}}_r)\\ &= \mathbf{s}^T(-\mathbf{K}\text{sign}(\mathbf{s}) + \mathbf{d})\\ &= -\mathbf{s}^T\mathbf{K}\text{sign}(\mathbf{s}) + \mathbf{s}^T\mathbf{d}\\ &= -\mathbf{K}_v|\mathbf{s}| + \mathbf{d}^T\mathbf{s}\end{aligned} \tag{24}$$

Here, $\mathbf{K}_v$ is a row vector containing the diagonal elements of the diagonal matrix $\mathbf{K}$. A bound is assumed for the elements of the 6×1 disturbance vector.

$$|d_i| \le D_i, \quad i = 1, \ldots, 6 \tag{25}$$

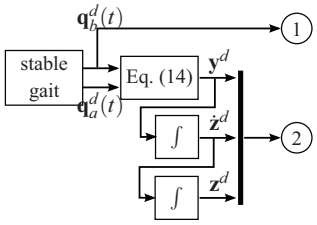

FIGURE 2. DESIRED OUTPUT SUBSYSTEM

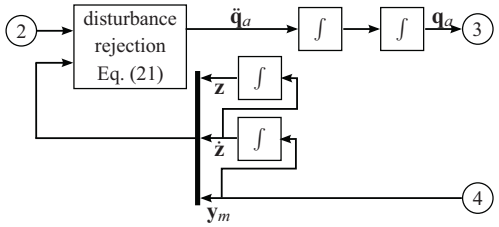

FIGURE 3. DISTURBANCE REJECTION SUBSYSTEM

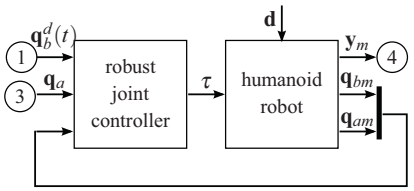

FIGURE 4. ROBOT JOINT CONTROL SUBSYSTEM

Equation (24) becomes

$$\begin{aligned}\dot{V} &\leq -\mathbf{K}_v|\mathbf{s}| + \mathbf{D}^T|\mathbf{s}|, \\ &\leq -(\mathbf{K}_v - \mathbf{D}^T)|\mathbf{s}|. \end{aligned} \tag{26}$$

Equation (26) implies that if the elements of $\mathbf{K}$ are selected such that they are larger than the corresponding elements of $\mathbf{D}^T$, rate of the Lyapunov function is negative, and $\mathbf{s}$ vanishes despite the existence of any disturbance less than or equal to $\mathbf{D}$. In other words,

$$\mathbf{K}_v \geq \mathbf{D}^T + \eta^T, \tag{27}$$

where η is a column vector with positive elements.

Complete Control Block Diagram

The complete control scheme consists of three subsystems, desired output, disturbance rejection, and robust joint control subsystems. In the following, these subsystems are discussed.

The subsystem that generates the desired outputs (i.e. support force and moment components) is shown in Fig. 2. First nominal trajectories are defined for the joints of the robot's arms ($\mathbf{q}_a^d(t)$), and legs and body ($\mathbf{q}_b^d(t)$). These trajectories are designed such that the requirements of a stable walk are met. These requirements are: a) The ZMP is confined in the support polygon during a walking cycle, and b) the longitudinal and lateral support forces and the support twist moment are lower than the static friction between the support foot and the ground. When these requirements are met, the corresponding support force and moment components ($\mathbf{y}^d$) yield a stable walk and are desirable. These desired support force and moment components are calculated using Eq. (14). Then, they are integrated using Eqs. (17) to provide additional variables needed for control.

The subsystem that modifies the arm motion ($\mathbf{q}_a$) to maintain the desired output ($\mathbf{y}_d$) in presence of possible disturbances is shown in Fig. 3. This subsystem is based on control law (21). It receives the desired output and its integrals from the desired output subsystem at junction 2, and the measured output ($\mathbf{y}_m$) and its integrals at junction 4. The measured output is provided by a shoe on the robot's foot, which is equipped with a number of force sensors with appropriate directions. The modified arm motion ($\mathbf{q}_a$) is the output of the disturbance rejection subsystem.

TABLE 1. ROBOT'S JOINT ANGLES AT THE START AND END OF A STEP IN DEGREES

	q_{b1}	q_{b2}	q_{b3}	q_{b4}	q_{a1}	q_{a2}	q_{a3}
Start	90	35	120	0	-50	210	150
End	65	0	240	325	10	210	150

The subsystem that controls the motion of the robot's joints is shown in Fig. 4. The the original desired motion of legs and body ($\mathbf{q}_b^d(t)$) and the modified arm motion ($\mathbf{q}_a$) are input to this subsystem at junctions 1 and 3, respectively. A robust joint controller (which is beyond the scope of this paper) calculates the required joint torques (τ) by receiving the measured joint positions ($\mathbf{q}_{am}$, $\mathbf{q}_{bm}$) and their derivatives (not shown on the figure for simplicity). The joint controller must be robust enough so that it perfectly performs the desired joint motion despite of the existence of a potential bounded disturbance.

Simulations

As an example, a 7-DOF biped robot is considered (Fig. 5). The degrees of freedom are the stance leg ankle joint (q_{b1}), the stance leg knee joint (q_{b2}), the hip joint between upper stance

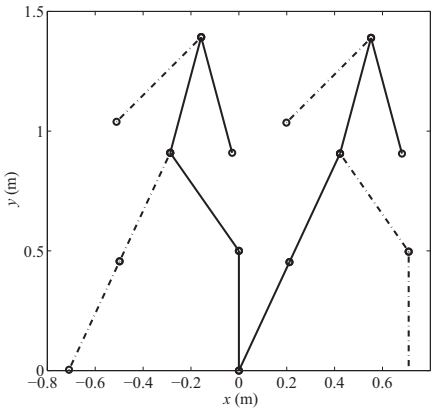

FIGURE 5. A 7-DOF BIPED ROBOT AT THE START AND END OF A STEP

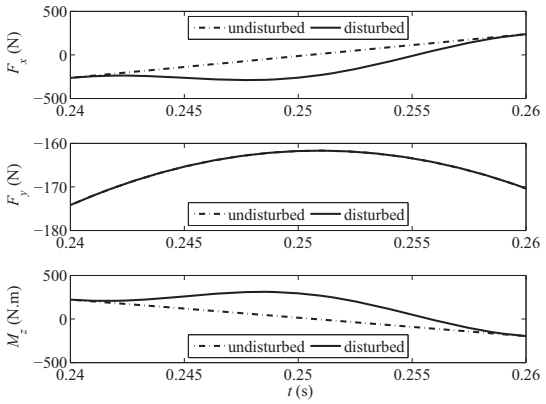

FIGURE 6. THE EFFECT OF THE DISTURBANCE ON THE SUPPORT FORCE, WHEN A DISTURBANCE REJECTION CONTROLLER IS NOT USED

leg and the upper swing leg (q_{b3}), the swing leg knee joint (q_{b4}), the hip joint between the upper stance leg and the body (q_{a1}), the shoulder joint of the right arm (q_{a2}), and the shoulder joint of the left arm (q_{a3}). The joint angles at the beginning and the end of the step are listed in Table 1. Seven-degree polynomials are used to plan the trajectory of the joints from start to the end of the step. Jerk, acceleration, and speed of the joints are zero at both the start and the end of the step. One step takes 0.5 seconds. All link lengths are assumed to be 0.5 meters, and each link has a mass of 10 kg.

In this example, it is assumed that the ZMP location and support forces corresponding to the defined desired trajectory are desirable. No attempt has been made to minimize the variation of the ZMP position for the defined walking gait. For simplicity, it is assumed that the feet of the robot are large enough to cover the variation of the ZMP position for the whole desired walking cycle of this robot. First, the desired joint trajectories are used to calculate the desired longitudinal force (F_x), vertical force (F_y), and lateral moment (M_z) that the robot exerts on the ground during a step. These forces and moments are valid when the robot walks in the absence of any external disturbances. In the presented graphs, these values are referred to as "undisturbed" values.

A disturbance is assumed to act on the robot from time 0.24 to 0.26 seconds, at the middle of 0.5-second step. The disturbance is a smooth varying horizontal force with a peak of 249 N (36.3% of the robot's weight) on the robot's body at a height of 1.125 m. This force also generates a moment about the foot that is on the ground. So, the disturbance vector has the following form.

$$\mathbf{d} = \begin{bmatrix} -249(1-\cos(\frac{2\pi(t-0.24)}{0.02}))/2 \\ 0 \\ 249(1.125)(1-\cos(\frac{2\pi(t-0.24)}{0.02}))/2 \end{bmatrix} \quad 0.24 \le t \le 0.26 \tag{28}$$

The effect of this disturbance on the support force, when a disturbance rejection controller is not used, is shown in Fig 6. This change in the support force could easily cause an unstable walk.

A disturbance rejection controller is designed that uses the acceleration of q_{a1}, q_{a2}, and q_{a3} as control inputs to control the support forces at the desired level equivalent to the case where no disturbance is present. That is, the motion of the arms and body are modified by the controller in real-time such that the support force/moment components are not affected. The effect of the disturbance on the support force, when a disturbance rejection controller is used, is shown in Fig 7. It is seen that the support force/moment components for the disturbed case almost exactly overlap those of the undisturbed case. When the support force/moment components are not affected by an external disturbance, the robot's walk remains stable despite of the disturbance.

The modified trajectory of the arms and the body are compared to the original ones in Fig. 8. A slight motion of the arms and a negligible motion of the body has been used by the controller to reject the disturbance.

The shift in the ZMP position is compared for both cases in Fig 9. The position of the ZMP is calculated by dividing M_z by F_y. The shift in the ZMP position is calculated by subtracting the ZMP position of the uncontrolled and controlled disturbed cases with that of the undisturbed case. It can be seen that the ZMP po-

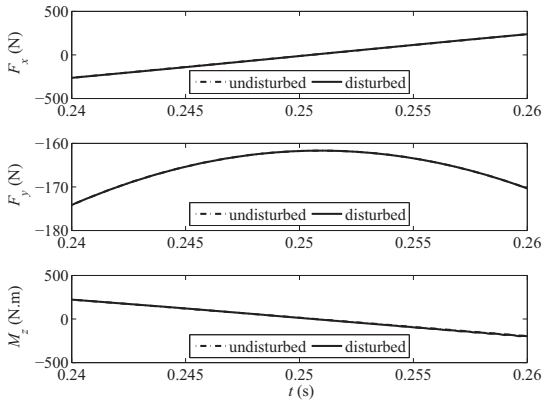

FIGURE 7. THE EFFECT OF THE DISTURBANCE ON THE SUPPORT FORCE, WHEN A DISTURBANCE REJECTION CONTROLLER IS USED

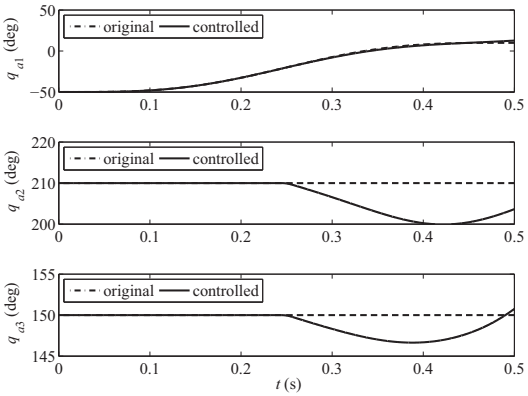

FIGURE 8. THE MODIFIED TRAJECTORY OF THE ARMS AND THE BODY COMPARED TO THE ORIGINAL ONES

sition has shifted close to 1.8 meters due to the large disturbance when the disturbance rejection controller is not used. This can easily cause the robot to lose its balance during the walk. The shift of the ZMP position is zero when the disturbance rejection controller is used. This means that if the original gait planned for the robot has a stable ZMP position, that ZMP position will be held by the disturbance rejection controller despite of the presence of a disturbance. So, the robot's walk will remain stable even when the disturbance is present.

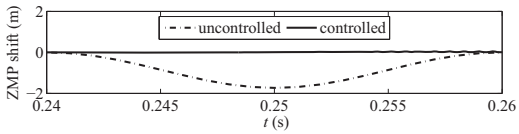

FIGURE 9. THE COMPARISON OF THE SHIFT IN THE ZMP FOR THE UNCONTROLLED AND CONTROLLED CASES

Conclusion

A disturbance rejection control approach is proposed for a biped humanoid with 6DOF per leg and 3DOF per arm. The swing phase of the robot's gait is considered. It is assumed that force sensors on the "shoe" of the robot provide the support forces and moments in real-time, and the position, velocity and acceleration of joints are available for feedback. A stable walking gait and arm movement with a desirable support force and moment distribution are defined. The disturbance rejection controller determines the arm joint accelerations in real-time to maintain the desirable support forces and moments despite bounded disturbances. Simulations show that, when the controller is used, support forces and moments remain at their desired values even if disturbance forces are exerted on the robot's body. The plot of the ZMP shift for the system with controller when a disturbance is applied shows no shift in the ZMP, which translates to the biped maintaining a stable gait despite the effect of the disturbance.

REFERENCES

[1] Vukobratovic, M., and Borovac, B., 2004. "Zero moment point - thirty five years of its life". *Int J Humanoid Robot,* ***1***(1), pp. 157–173.

[2] R. Zhang, P. V., and Chew, C. M., 2003. "Motion planning for biped robot climbing stairs". In Proceeding of FIRA Robot World Congress.

[3] K. Hirai, M. Hirose, Y. H., and Takenaka, T., 1998. "The development of Honda humanoid robot". In Proceedings of the 1998 IEEE International Conference on Robotics and Automation, Vol. 2, pp. 1321–1326.

[4] Vadakkepat Prahlad, G. D., and Meng-Hwee, C., 2008. "Disturbance rejection by online ZMP compensation". *Robotica,* ***26***, pp. 9–17.

[5] Okumura, Y., Tawara, T., Endo, K., Furuta, T., and Shimizu, M., 2003. "Real-time ZMP compensation for biped walking robot using adaptive inertia force control". In Proceedings 2003 IEEE/RSJ International Conference on Intelligent Robots and Systems (IROS 2003), Vol. 1, pp. 335–339.

[6] H. O. Lim, Y. K., and Takanishi, A., 2002. "Online walking pattern generation for biped humanoid robot with trunk". In

Proceedings of IEEE International Conference on Robotics and Automation, Vol. 3, pp. 3111–3116.
[7] J. Yamaguchi, E. Soga, S. I., and Takanishi, A., 1999. "Development of a bipedal humanoid robot-control method of whole body cooperative dynamic biped walking". In Proceedings of 1999 IEEE International Conference on Robotics and Automation, Vol. 1, pp. 368–374.
[8] K. Mitobe, G. C., and Nasu, Y., 2000. "Control of walking robots based on manipulation of the zero moment point". *Robotica,* ***18***(6), pp. 651–657.
[9] Park, J. H., and Chung, H., 1999. "ZMP compensation by online trajectory generation for biped robots". In Proceedings of IEEE International Conference on Robotics and Automation, Vol. 4, pp. 960–965.
[10] Kajita, S., 2003. "Biped walking pattern generation by using preview control of zero-moment point". In Proceeding of IEEE International Conference on Robotics and Automation, Vol. 2, pp. 1620–1626.
[11] Hammam, G. B., Orin, D., and Dariush, B., 2010. "Whole-body humanoid control from upper-body task specifications". In Proceedings of 2010 IEEE International Conference on Robotics and Automation (ICRA), pp. 3398 – 3405.
[12] Hofmann, A., Massaquoi, S., Popovic, M., and Herr, H., 2004. "A sliding controller for bipedal balancing using integrated movement of contact and non-contact limbs". In Proceedings of 2004 IEEE/RSJ International Conference on Intelligent Robots and Systems (IROS), Vol. 2, pp. 1952 – 1959.

REFERENCES

[1] Tad McGeer. Passive dynamic walking. *International Journal of Robotics Research*, 9(2):62 – 82, 1990.

[2] Zhenze Liu, Aichun Zhang, Yantao Tian, Peijie Zhang, and Dengfeng Gao. Further analysis of the kneed passive-dynamic biped robot. In *2010 Chinese Control and Decision Conference, CCDC 2010*, pages 1777 – 1782, Xuzhou, China, 2010.

[3] Kentarou Hitomi, Tomohiro Shibata, Yutaka Nakamura, and Shin Ishii. Reinforcement learning for quasi-passive dynamic walking of an unstable biped robot. *Robotics and Autonomous Systems*, 54(12):982 – 988, 2006.

[4] Myriam Ferry, Luc Martin, Nicolas Termoz, Julie Cote, and Francois Prince. Balance control during an arm raising movement in bipedal stance: Which biomechanical factor is controlled? *Biological Cybernetics*, 91(2):104 – 114, 2004.

[5] Fu Chunqian and Wang Xingsong. Force-shoes ZMP measuring system for human walker. In *15th International Conference on Mechatronics and Machine Vision in Practice, M2VIP'08*, pages 527 – 532, Auckland, New Zealand, 2008.

[6] M. Vukobratovic and B. Borovac. Zero moment point - thirty five years of its life. *Int J Humanoid Robot*, 1(1):157–173, 2004.

[7] P. Vadakkepat R. Zhang and C. M. Chew. Motion planning for biped robot climbing stairs. In *Proceeding of FIRA Robot World Congress*, Vienna, Austria, Oct. 1-3, 2003.

[8] Y. Haikawa K. Hirai, M. Hirose and T. Takenaka. The development of Honda humanoid robot. In *Proceedings of the 1998 IEEE International Conference on Robotics and Automation*, volume 2, pages 1321–1326, 1998.

[9] Goswami Dip Vadakkepat Prahlad and Chia Meng-Hwee. Disturbance rejection by online ZMP compensation. *Robotica*, 26:9–17, 2008.

[10] Nirut Naksuk, C. S. George Lee, and Shirley Rietdyk. Whole-body human-to-humanoid motion transfer. In *Proceedings of 2005 5th IEEE-RAS International Conference on Humanoid Robots*, volume 2005, pages 104 – 109, Tsukuba, Japan, 2005.

[11] A. Sano and J. Furusho. Realization of natural dynamic walking using the angular momentum information. In *Robotics and Automation, 1990. Proceedings., 1990 IEEE International Conference on*, volume 3, pages 1476 –1481, May 1990.

[12] Y. Okumura, T. Tawara, K. Endo, T. Furuta, and M. Shimizu. Real-time ZMP compensation for biped walking robot using adaptive inertia force control. In *Proceedings 2003 IEEE/RSJ International Conference on Intelligent Robots and Systems (IROS 2003)*, volume 1, pages 335–339, Piscataway, NJ, USA, 2003.

[13] Ill-Woo Park, Jung-Yup Kim, and Jun-Ho Oh. Online biped walking pattern generation for humanoid robot KHR-3(KAIST humanoid robot - 3: HUBO). In *Proceedings of the 2006 6th IEEE-RAS International Conference on Humanoid Robots, HUMANOIDS*, pages 398 – 403, Genoa, Italy, 2006.

[14] Ill-Woo Park, Jung-Yup Kim, and Jun-Ho Oh. Online walking pattern generation and its application to a biped humanoid robot - KHR-3 (HUBO). *Advanced Robotics*, 22(2-3):159 – 190, 2008.

[15] Y. Kaneshima H. O. Lim and A. Takanishi. Online walking pattern generation for biped humanoid robot with trunk. In *Proceedings of IEEE International Conference on Robotics and Automation*, volume 3, pages 3111–3116, 2002.

[16] S. Inoue J. Yamaguchi, E. Soga and A. Takanishi. Development of a bipedal humanoid robot-control method of whole body cooperative dynamic biped walking. In *Proceedings of 1999 IEEE International Conference on Robotics and Automation*, volume 1, pages 368–374, 1999.

[17] G. Capi K. Mitobe and Y. Nasu. Control of walking robots based on manipulation of the zero moment point. *Robotica*, 18(6):651–657, 2000.

[18] J. Vermeulen, B. Verrelst, D. Lefeber, P. Kool, and B. Vanderborght. A real-time joint trajectory planner for dynamic walking bipeds in the sagittal plane. *Robotica*, 23(6):669 – 680, 2005.

[19] J. H. Park and H. Chung. ZMP compensation by online trajectory generation for biped robots. In *Proceedings of IEEE International Conference on Robotics and Automation*, volume 4, pages 960–965, Oct. 10-15, 1999.

[20] Tomomichi Sugihara, Yoshihiko Nakamura, and Hirochika Inoue. Realtime humanoid motion generation through ZMP manipulation based on inverted pendulum control. In *Proceedings - IEEE International Conference on Robotics and Automation*, volume 2, pages 1404 – 1409, Washington, DC, United States, 2002.

[21] Kemalettin Erbatur and Okan Kurt. Humanoid walking robot control with natural ZMP references. In *IECON Proceedings (Industrial Electronics Conference)*, pages 4100 – 4106, Paris, France, 2006.

[22] Shuuji Kajita, Fumio Kanehiro, Kenji Kaneko, Kazuhito Yokoi, and Hirohisa Hirukawa. The 3D linear inverted pendulum mode: A simple modeling for a biped walking pattern generation. In *IEEE International Conference on Intelligent Robots and Systems*, volume 1, pages 239 – 240, Maui, HI, United States, 2001.

[23] Bum-Joo Lee, Daniel Stonier, Yong-Duk Kim, Jeong-Ki Yoo, and Jong-Hwan Kim. Modifiable walking pattern generation using real-time ZMP manipulation for humanoid robots. In *IEEE International Conference on Intelligent Robots and Systems*, pages 4221 – 4226, San Diego, CA, United States, 2007.

[24] G. Bin Hammam, D.E. Orin, and B. Dariush. Whole-body humanoid control from upper-body task specifications. In *Proceedings of 2010 IEEE International Conference on Robotics and Automation (ICRA)*, pages 3398 – 3405, 3-7 May 2010.

[25] Andreas Hofmann, Steven Massaquoi, Marko Popovic, and Hugh Herr. A sliding controller for bipedal balancing using integrated movement of contact and non-contact limbs. In *Proceedings of 2004 IEEE/RSJ International Conference on Intelligent Robots and Systems (IROS)*, volume 2, pages 1952 – 1959, Sendai, Japan, 2004.

[26] Weiping Li Jean-Jacques E. Slotine. *Applied Nonlinear Control*. Prentice Hall, 1991.

[27] Jaeheung Park. Synthesis of natural arm swing motion in human bipedal walking. *Journal of Biomechanics*, 41(7):1417 – 1426, 2008.

[28] C. Zaoui, O. Bruneau, F.B. Ouezdou, and A. Maalej. Simulations of the dynamic behavior of a bipedal robot with trunk and arms subjected to 3D external disturbances in a vertical posture, during walking and during object handling. *Multibody System Dynamics*, 21(3):261 – 280, 2009.

[29] Chen-Bo Yin, Qing-Min Zhou, Hai-Han Xu, and Min Yang. Stability maintenance of a humanoid robot under extern disturbance. *Kongzhi yu Juece/Control and Decision*, 21(6):619 – 624, 2006.

[30] Makoto Shimojo, Takuma Araki, Aigou Ming, and Masatoshi Ishikawa. A ZMP sensor for a biped robot. In *Proceedings - IEEE International Conference on Robotics and Automation*, volume 2006, pages 1200 – 1205, Orlando, FL, United States, 2006.

[31] John J. Craig. *Introduction to Robotics: Mechanics and Control*. Prentice Hall, 3rd edition, 2005.

[32] ROBOTIS, 2006. Dynamixel AX-12 User's Manual.

[33] Farbod Fahimi and Joshua Hill. Active disturbance rejection for bipedal walk of a humanoid robot using the motions of the arms. In *2011 ASME International Mechanical Engineering Congress and Exposition*, Denver, CO, 2011.